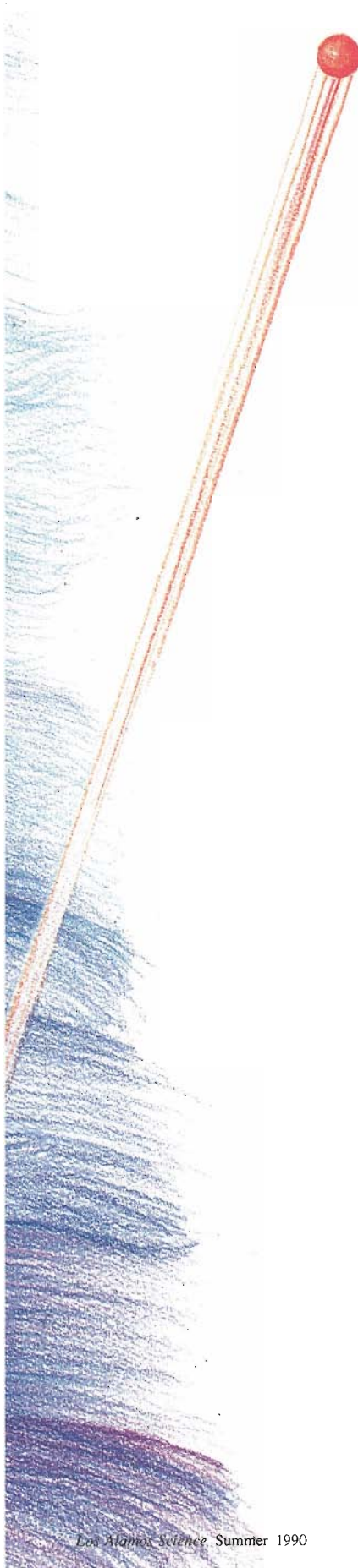


A fanciful view of an atom in superfluid helium-4 (blue) being struck by a neutron (red) and then bouncing off the interaction potentials of neighboring atoms. These so-called final-state interactions prevent direct observation of the Bose condensate—the exotic state of matter whose existence was proposed in 1938 by Fritz London as an explanation of superfluidity. Although the rune above, by E. C. Svensson, appeared in 1983 (in *75th Jubilee Conference on Helium-4*), its claim was only recently confirmed.



superfluid helium and neutron scattering a new chapter in the CONDENSATE SAGA

by Richard N. Silver

The unusual properties of helium at temperatures near absolute zero have been an endless source of fascination for condensed-matter physicists. Helium is the only atomic system that avoids crystallization and instead remains a fluid to arbitrarily low temperature. Moreover, when a liquid composed of ^4He atoms is cooled below a critical temperature T_λ (equal to 2.17 kelvins at atmospheric pressure), it passes from a *normal-fluid* state, so called because its properties are similar to those of other fluids, to a *superfluid* state having dramatically different properties. A normal fluid possesses a finite viscosity, or resistance to shear flow, and therefore current flows dissipate in the absence of a driving force. A normal fluid also has a finite thermal conductivity, or the ability to support temperature gradients. In contrast, a superfluid has a zero viscosity and an infinite thermal conductivity. In a superfluid quantized currents persist indefinitely, and temperature fluctuations propagate like waves. In addition, numerous other properties of superfluids lie outside the realm of common experience. Finally, unlike the behavior of normal fluids, which can usually be described in terms of classical mechanics, the exotic behavior of liquid helium below T_λ requires a quantum-mechanical description. For that reason superfluid helium is called a *quantum fluid*.

In this article we focus on a single question: What quantum features of helium atoms at temperatures below T_λ might explain the transition from normal-fluid to superfluid behavior? We shall eventually arrive at a clear answer, but the route we must follow to find it is circuitous. Along the way we will explore much of the history of and current research on quantum fluids and learn about related research in many areas of modern physics. We will see that the high fluxes of epithermal neutrons available at pulsed neutron sources, such as those at Argonne and Los Alamos National Laboratories, are a powerful tool in addressing our central question.

An important clue to the answer comes from comparing the behavior of two different helium fluids, one composed of ^3He atoms and the other of ^4He atoms. Both isotopic species have identical interatomic interactions, and the difference in their masses has a negligible effect on their behavior. Under atmospheric pressure both remain fluids to arbitrarily low temperatures. However, ^4He undergoes a superfluid transition at 2.17 kelvins, but ^3He does not become a superfluid until below 3 millikelvins. The transition temperatures of the two species differ by three orders of magnitude!

The origin of that great difference can be traced to the *spin-statistics relation*, the fundamental principle of quantum mechanics that distinguishes ^3He from ^4He . *Statistics* refers to symmetry properties of the wave function describing a system of identical (and therefore indistinguishable) particles. The ^3He nucleus, composed

of two protons and one neutron, has a spin of $\frac{1}{2}$; that is, it has an intrinsic angular momentum of $\frac{1}{2}\hbar$, where \hbar is Planck's constant divided by 2π . (Electrons also have a spin of $\frac{1}{2}$, but the spins of the two electrons in each helium atom are antiparallel and thus contribute a total spin of zero.) According to the spin-statistics relation, a system of identical particles having half-integer spin must be described by a many-particle wave function that is a completely antisymmetric function of the particle positions. Such a function is zero when two particles have the same position. Therefore, since the probability of finding particles at given positions is the square of the wave function, the spin-statistics relation alone requires particles with half-integer spin to avoid one another even in the absence of any repulsive potential between them. The antisymmetry of the wave function is thus the origin of the famous Pauli exclusion principle, which requires that no two electrons in an atom occupy the same atomic orbital. (Particles with half-integer spin are termed *fermions*, and the spin-statistics relation for fermions is called Fermi-Dirac statistics.)

The converse is true for ^4He atoms. The ^4He nucleus, composed of two protons and two neutrons, has a spin of 0, and so also does the ^4He atom. According to the same spin-statistics relation, a system of identical particles having integer spin must be described by a many-particle wave function that is a completely symmetric function of the particle positions. A completely symmetric function is larger when two particles occupy the same position. Hence, the spin-statistics relation requires integer-spin particles, such as spin-0 ^4He atoms and spin-1 photons, to be attracted to one another even in the absence of any attractive potential between them. (Particles with integer spin are termed *bosons*, and the spin-statistics relation for bosons is called Bose-Einstein statistics.)

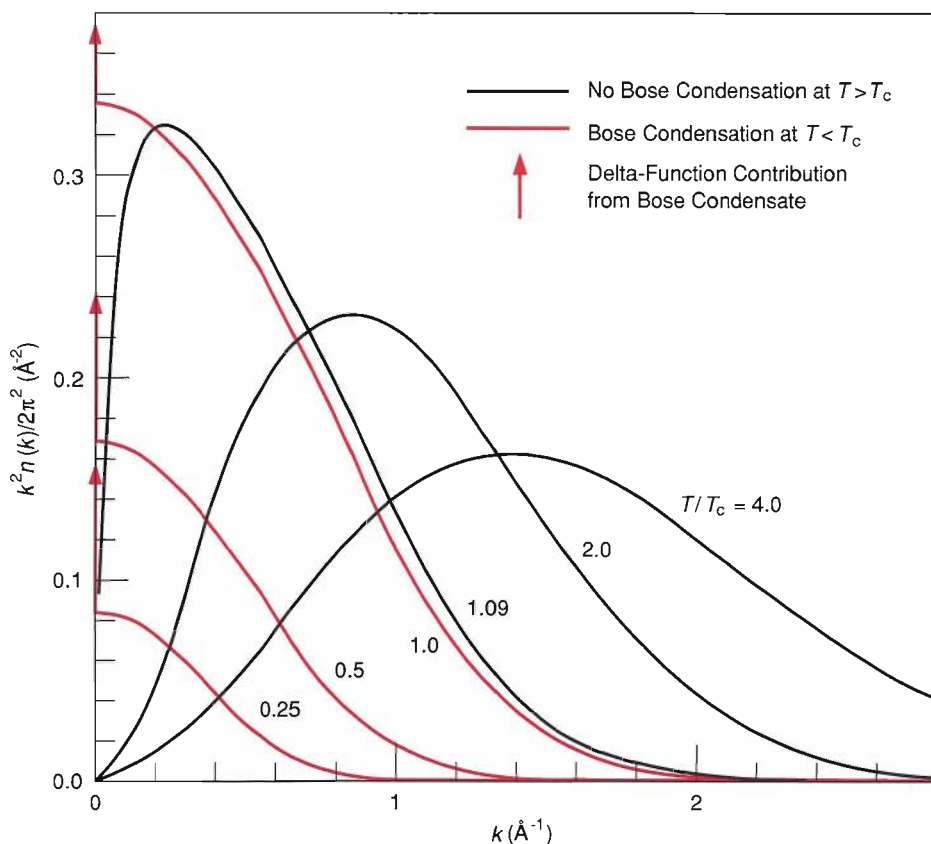
Although the spin-statistics relation applies to the *microscopic* behavior of a system of identical particles, its effects are visible at the human, or *macroscopic*, level of perception. For example, if all the electrons in an atom could occupy the lowest atomic orbital, then the universe as we know it would collapse. Fortunately electrons are fermions, and such a collapse is forbidden by the Pauli exclusion principle. An outstanding macroscopic effect for bosons is the phenomenon of lasing. A laser can produce an intense beam of coherent light because the photons emitted by a large population of excited atoms are allowed, and indeed prefer, to enter the same quantum-mechanical state.

In 1938 Fritz London proposed that the superfluidity observed in liquid ^4He earlier that year was just such a macroscopic manifestation of the symmetry requirement for the wave function of a system of identical bosons, an insight that preceded the invention of lasers by twenty-seven years. He reasoned by analogy with the theoretically predicted behavior of a non-interacting gas of spin-0 particles obeying Bose-Einstein statistics. His argument is given in terms of the momentum wave function of the system, which is simply the Fourier transform of the position wave function mentioned above. (Position and momentum are expressed mathematically in quantum mechanics as Fourier conjugate variables that obey the Heisenberg uncertainty principle, $\Delta p \Delta x \leq \hbar$, where Δp and Δx are the uncertainties in momentum and position.)

Consider a system of identical atoms inside a box of finite size. The probability that an atom has momentum of magnitude p in, say, the x direction is termed the *momentum distribution*, $n(p)$. For all systems of atoms obeying classical mechanics, $n(p)$ is given by a Maxwell-Boltzmann distribution, which is a Gaussian function of width $\Delta p = \sqrt{mk_{\text{B}}T}$ in each direction. Here m is the atomic mass, k_{B} is Boltzmann's constant, and T is temperature. This classical-mechanical momentum distribution is independent of any interactions between the atoms and yields an average kinetic, or thermal, energy ($\propto (\Delta p)^2/2m$) per atom of $\frac{3}{2}k_{\text{B}}T$. Thus, all liquids that obey classical mechanics must crystallize as the temperature is lowered because the potential energy gained by the localization of atoms at lattice sites overcomes the kinetic energy due to thermal motion. That ^4He and ^3He require a quantum description is already

MOMENTUM DISTRIBUTIONS IN AN IDEAL BOSE GAS

Fig. 1. Shown here are plots, at various temperatures above and below the Bose-condensation temperature T_c , of $k^2 n(k)/2\pi^2$ versus k , where $n(k)$ is the momentum distribution of an ideal Bose gas of density ρ . As the temperature decreases toward T_c , $k^2 n(k)$ deviates more and more from the classical prediction of a (Gaussian) Maxwell-Boltzmann momentum distribution. At temperatures below T_c , a nonzero fraction $n_0(T)$ of the bosons occupies the zero-momentum state, and $n(k)$ includes a delta-function contribution equal to $n_0(T)\rho(2\pi)^3\delta(k)$. Thus $k^2 n(k)$ increases as k approaches 0 and exhibits a positive discontinuity at $k = 0$.

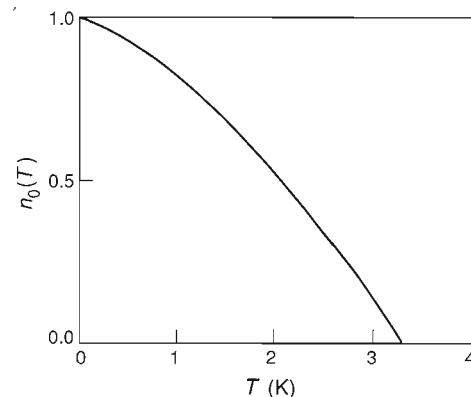


evident from the fact that they remain liquid all the way down to absolute zero.

In quantum mechanics the momenta of atoms in a finite-sized box are quantized in integer multiples of $\hbar L^{-1}$, where L is a dimension of the box. This quantization is a consequence of the requirement that the wave function of an atom must be zero at the boundaries of the box and therefore must have an integral number of nodes. Thus the momentum distribution for the system is discontinuous (unlike the continuous Maxwell-Boltzmann distribution of classical systems) and becomes continuous only for a box of infinite size.

Now consider the momentum distribution for a non-interacting (ideal) gas of spin-0 atoms. At high temperature the atoms are thermally excited, and the probability of an atom being in any particular momentum state is inversely proportional to the size of the system (L^3) and proportional to a Maxwell-Boltzmann distribution. However, as the temperature is reduced, the preference of bosons for occupying the same momentum state causes deviations from the Maxwell-Boltzmann distribution. As the temperature is further reduced below a critical *Bose-condensation temperature*, a significant fraction of the atoms begin to occupy the lowest (or zero) momentum state. The fraction, n_0 , is called the Bose-condensate fraction, and its value is independent of the size of the system. In the momentum distribution n_0 shows up as a delta function, of weight n_0 , at $p = 0$. The width Δp of the momentum distribution for the remainder of the atoms is on the order of $\sqrt{mk_B T}$ and goes to zero at zero temperature. On the other hand, n_0 approaches one as the temperature approaches zero; that is, the entire system becomes a Bose condensate. Figure 1 shows plots of $k^2 n(k)$ versus k for a system of non-interacting bosons at various temperatures. (In this article momentum \mathbf{p} and the wave vector $\mathbf{k} \equiv \mathbf{p}/\hbar$ are used interchangeably. The natural unit for wave-vector magnitudes is the inverse angstrom, \AA^{-1} .) Figure 2 is a plot of the Bose-condensate fraction n_0 versus temperature.

London reasoned that the superfluidity observed in ^4He was a macroscopic consequence of the microscopic Bose condensation of ^4He atoms into the zero-

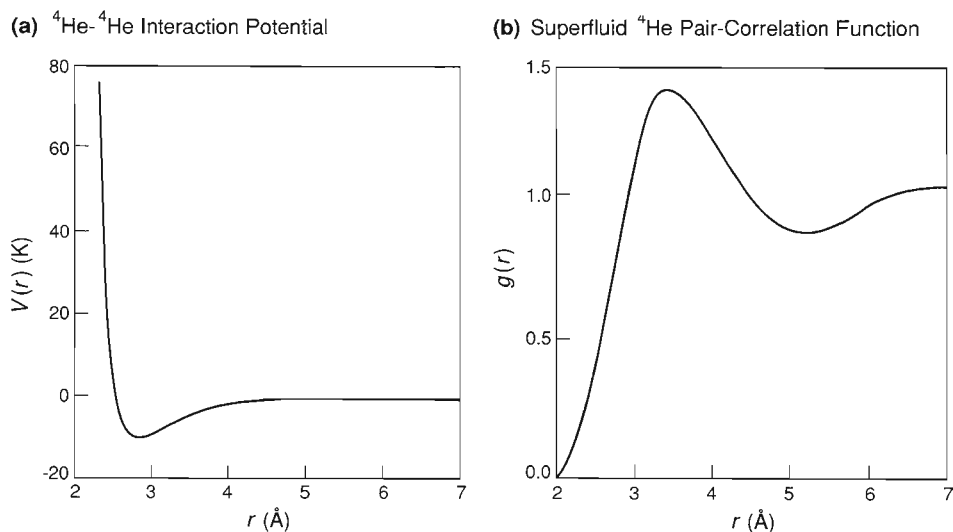


BOSE-CONDENSATE FRACTION IN AN IDEAL BOSE GAS

Fig. 2. The Bose-condensate fraction in an ideal Bose gas with a density equal to that of liquid ^4He increases monotonically from 0 at its Bose-condensation temperature (3.3 kelvins) to 1 at absolute zero.

DEPARTURE OF LIQUID ^4He FROM IDEAL-GAS BEHAVIOR

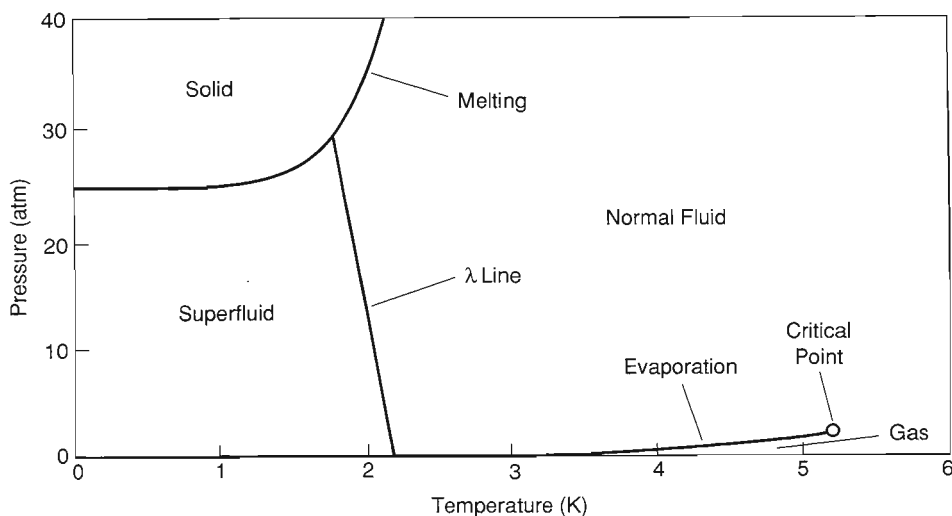
Fig. 3. (a) The potential $V(r)$ for the interaction between atoms in liquid ^4He is steeply repulsive (positive) at interatomic distances below about 2.6 angstroms. At larger distances van der Waals forces cause the potential to be weakly attractive (negative). Such an interaction potential, which differs enormously from that of an ideal gas, leads to spatial correlations between the atoms in liquid ^4He . (b) Shown here is the pair-correlation function $g(r)$ for superfluid ^4He determined by neutron diffraction. It is proportional to the probability distribution for finding two atoms of superfluid ^4He a distance r apart. Comparison of $g(r)$ and $V(r)$ reveals that the atoms in the superfluid tend to stay in the attractive well of the potential, outside its steeply repulsive core.



momentum state. He pointed out that the Bose-condensation temperature of a system of non-interacting atoms having the same mass and density as ^4He is 3.3 kelvins and is thus remarkably close to the observed ^4He superfluid-transition temperature of 2.17 kelvins. London's hypothesis also suggests why liquid ^3He behaves so differently from liquid ^4He at low temperature: The spin-statistics relation for fermions forbids Bose condensation of ^3He atoms. London's analogy between ^4He and a system of non-interacting bosons is imperfect because the atoms in liquid helium interact strongly. Such interatomic interactions have a significant effect on the momentum distribution of a quantum system. As shown in Fig. 3a, the interaction potential between ^4He atoms is strongly repulsive at interatomic distances less than 2.5 angstroms and weakly (van der Waals) attractive at larger distances. Therefore the atoms tend to stay a minimum of 2.5 angstroms apart. Indeed, as shown in Fig. 3b, the pair-correlation function, $g(r)$, for liquid ^4He (which is proportional to the probability distribution for finding two ^4He atoms a distance r apart) has a maximum at about 3.5 angstroms. Now, since liquid helium is a quantum system obeying the Heisenberg uncertainty principle, the correlation in the positions of the the atoms must result in a spread in the probability of their occupying any of the momentum states. In particular, the tendency of ^4He atoms to stay at least 2.5 angstroms apart results in an expected width of the momentum distribution of $\Delta k = (2\pi/2.5) \text{ \AA}^{-1}$, or about 2 \AA^{-1} . Thus, even at absolute zero interacting atoms have a finite kinetic energy of $(\hbar\Delta k)^2/2m$, which is termed the *zero-point energy*. The uncertainty in the atom's momentum increases its kinetic energy above the classical value at any temperature.

For most atomic systems the zero-point energy is too small to prevent crystallization at low temperatures. The only exceptions are ^4He and ^3He . At pressures below tens of atmospheres, helium atoms tend to sit in the shallow potential well created by the weakly attractive van der Waals force, but their comparatively low masses result in zero-point kinetic energies that are higher than the van der Waals potential energy. Only at very high densities are the atoms close enough that their potential energy due to the steeply repulsive part of the potential exceeds the zero-point energy and produces crystallization. Thus the low-temperature phase diagram for ^4He (Fig. 4) shows crystallization above 25 atmospheres. At lower pressures ^4He remains a liquid down to absolute zero. Moreover, along the so-called λ line ^4He undergoes the phase transition from the normal to the superfluid state.

The really daring aspect of London's hypothesis was to propose that, despite the strong interactions between ^4He atoms, which tend to broaden the momentum distribution, the superfluid should contain a non-negligible fraction of atoms in the zero-momentum state. The remaining atoms should have a broad momentum distribution



PHASE DIAGRAM OF ${}^4\text{He}$

Fig. 4. At pressures below 25 atmospheres, the zero-point energy of liquid ${}^4\text{He}$ is sufficiently large to prevent its solidification, even at a temperature of absolute zero. The liquid phase is separated by the λ line into normal-fluid and superfluid phases. At atmospheric pressure the superfluid-transition temperature T_λ is 2.17 kelvins, which is not much different from the Bose-condensation temperature of an ideal Bose gas of the same density (3.3 kelvins). The critical point shown in the phase diagram gives the pressure and temperature at which the liquid and gas phases of ${}^4\text{He}$ form one phase.

that remains wide (about 2 \AA^{-1}) even at zero temperature because of zero-point motion. (Superfluid flow is attributed to Bose condensation into a state other than the zero-momentum state. Coherent interactions among the ${}^4\text{He}$ atoms stabilize the flow against scattering processes, which tend to dissipate flow in normal fluids.)

London's hypothesis began what has been called the *condensate saga*—the story of numerous attempts by theorists to calculate the Bose-condensate fraction and by experimentalists to measure it. The condensate fraction has been elusive, and the saga has had many twists and turns. Both the existence and the size of the Bose-condensate fraction in superfluid ${}^4\text{He}$ have remained very controversial subjects. Most of the successful theories of superfluid helium (developed by, among others, Lev Landau, L. Tisza, and London) do not invoke a many-atom wave function at a microscopic level and especially not a Bose condensate. Rather, most of the remarkable properties of superfluid helium can be explained by the *two-fluid* model in which a macroscopic wave function extending throughout the sample corresponds to the superfluid component of the fluid, and elementary excitations out of the superfluid state, the so-called *phonons* and *rotons*, correspond to the normal component of the fluid. At zero temperature all the atoms are condensed into the macroscopic wave function, and helium consists entirely of superfluid. As the temperature is raised above zero, the number of thermally excited phonons and rotons increases, and they act as a normal fluid component. At T_λ , where the number of thermally excited elementary excitations equals the number of atoms in the system, the entire system becomes a normal fluid. This two-fluid description can account successfully for many experiments on superfluid ${}^4\text{He}$. Thus establishing a theoretical connection between the two-fluid model and the many-atom wave function is unnecessary to successful prediction of most macroscopic experiments. However, a goal of microscopic (atomic level) theory has been to predict the parameters of the two-fluid model, now obtained by fitting the model to macroscopic experiments. Until we achieve such a connection between the microscopic and macroscopic theories, we cannot determine n_0 from macroscopic experiments.

Nevertheless, many theorists over the years have spent an enormous effort on the microscopic theory of superfluid ${}^4\text{He}$. One goal has been to calculate n_0 , and indeed the entire momentum distribution, from first principles (*ab initio*) and the measurable interatomic potential. In addition to scientists' gut-level "need-to-know," many other factors motivate this enterprise. Helium is arguably the simplest among a wide variety of strongly interacting many-body systems currently under intense study by condensed-matter physicists. Those systems relate to such fashionable topics as high-temperature superconductors, heavy-fermion metals, the quantized Hall effect, and so on. Countless theoretical methods developed for and tested on helium have

subsequently provided the key to understanding more complex systems. Also, superfluidity in helium shares many similarities with superconductivity in metals, so that work on helium can be directly related to technologically important questions. Finally, the microscopic theory of helium, one of the most strongly interacting many-body systems, presents a fundamental challenge.

Progress in *ab initio* many-body calculations of the properties of liquid helium has been dramatic, especially since the advent of supercomputers in the last decade. The names of the methods employed are characteristically arcane (variational wave function, Green's function Monte Carlo, and path-integral Monte Carlo, for example) and reflect their great diversity. Nevertheless, the results of all these methods have converged on the conclusion that the Bose-condensate fraction should exist in superfluid ^4He but not in the normal fluid and that its value should be about 10 percent at zero temperature. Hence, measurements of n_0 provide a fundamental test of the predictive power of modern condensed-matter theory.

A seminal suggestion made by P. Hohenberg and P. Platzman in 1966 still remains the best hope for a direct measurement of momentum distributions in liquid helium. It involves neutron-scattering experiments at momentum and energy transfers sufficiently high that the struck atoms acquire kinetic energies much larger than the binding energies in the liquid. Under such conditions (hopefully!) the *impulse approximation*, which approximates the scattering from the many-atom system as the sum of scatterings from individual free atoms, is valid, and the observed scattering cross section is a direct measure of the momentum distribution in the sample. Analogous experiments are of interest in all of modern physics because momentum distributions are measurable properties of all many-particle wave functions, provided the energy and momentum transfers are high enough. X-ray Compton scattering at energies on the order of tens of keV can measure electron momentum distributions in atoms and solids, electron scattering at a few GeV can measure nucleon momentum distributions in nuclei, and electron scattering at hundreds of GeV can measure quark momentum distributions in nucleons. Scattering at very high energy transfers relative to the binding energies of a system is called *deep inelastic scattering*.

The suggestion of Hohenberg and Platzman initiated an effort that has lasted more than twenty years and has involved over one hundred experimentalists at reactor and pulsed neutron sources all over the world. The effort has spawned improvements in spectrometers and advances in data-analysis procedures. The attempted momentum-distribution measurements have used neutrons with energies between 10 and 1000 meV. Increases in neutron energy have been made in order to come closer to the regime in which the impulse approximation is valid. The goal of inferring the value of n_0 from the data inevitably involves accounting for instrumental broadening, statistical and background uncertainties, and corrections to the impulse approximation necessitated by the finite neutron energies available. Although the condensate saga through 1987 included many (often conflicting) indirect determinations of n_0 , it did not include any direct observation of the delta function in the momentum distribution of superfluid ^4He predicted by the London theory. Direct experimental evidence for a Bose condensate in superfluid helium was weak.

This article presents the latest episode in the condensate saga—a recent breakthrough in confirming the existence and size of the Bose-condensate fraction. New experiments using the high epithermal flux of a pulsed neutron source are in excellent agreement with sophisticated new *ab initio* calculations of momentum distributions, provided that the prediction of the impulse approximation is broadened by final-state interactions according to a first-principles theory developed by the author. Experiment and theory on the momentum distributions of ^4He have converged, and both are consistent with a condensate fraction of 9.2 percent in the superfluid at zero temperature. The story of the breakthrough is accompanied by a discussion of its implications for the study of other condensed-matter systems.

Neutron Scattering and the Impulse Approximation

As mentioned above, the best hope for measuring momentum distributions in helium is neutron scattering at high momentum and energy transfers. To understand why, let's review what we learn from neutron-scattering experiments (see also "Neutron Scattering—A Primer" in this issue). The double differential scattering cross section, or the scattering per unit solid angle Ω and per unit energy transfer $\hbar\omega$, is defined as

$$\frac{d^2\sigma}{d\omega d\Omega} \equiv \frac{\sigma_{\text{total}}^n k_i}{4\pi k_f} S(Q, \omega), \quad (1)$$

where σ_{total}^n is the total neutron-scattering cross section of a single helium atom, \mathbf{k}_i and \mathbf{k}_f are the initial and final neutron wave vectors, the energy transfer $\hbar\omega = (\hbar^2/2m_n)(k_i^2 - k_f^2)$, m_n is the neutron mass, $\hbar\mathbf{Q} \equiv \hbar|\mathbf{k}_i - \mathbf{k}_f|$ is the momentum transfer, and $S(Q, \omega)$ is the *dynamic structure factor* (also sometimes termed the *neutron scattering law*).

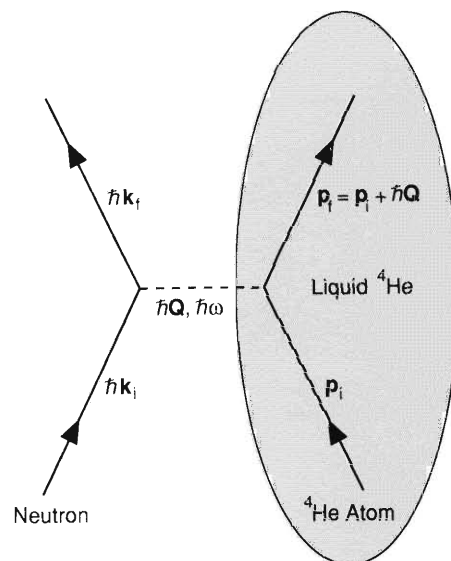
As discussed in the primer, $S(Q, \omega)$ is the Fourier frequency and spatial transform of the time-dependent pair-correlation function of the liquid. Measurement of $S(Q, \omega)$ provides a rich variety of information on the properties of quantum fluids. By the uncertainty principle experiments at Q values smaller than or comparable to the inverse of the interatomic spacing (that is, at $Q \leq$ a few \AA^{-1}) are sensitive to the collective behavior of helium atoms. For example, *diffraction* experiments, which involve elastic scattering ($k_i = k_f$), yield the *static structure factor* $S(Q) \equiv \int d(\hbar\omega) S(Q, \omega)$. The Fourier transform of $S(Q)$ for ${}^4\text{He}$ yields the pair-correlation function shown in Fig. 3b. And experiments involving *inelastic* scattering ($k_i \neq k_f$) at low Q determine the spectrum of elementary excitations (phonons and rotons) in ${}^4\text{He}$.

On the other hand, inelastic-scattering experiments at Q values much larger than a few \AA^{-1} probe individual atoms rather than collective behavior. That fact led to Hohenberg and Platzman's suggestion for using such experiments to measure the momentum distributions in helium. They assumed, first, that if the energy transfer is large compared to typical binding energies in the condensed phase (which are on the order of meV), then the initial binding energy of the atoms could be ignored, and second, that if the energy transfer is very large compared to the potential energy of the scattered atoms in the condensed phase, then a struck atom in its final state will be negligibly affected by the surrounding atoms and may be considered to be a free particle. Those assumptions imply that neutron scattering at very high energy and momentum transfers may be approximated as scattering from a collection of free helium atoms with initial momenta \mathbf{p}_i distributed according to the momentum distribution $n(\mathbf{p}_i)$ and with final momenta $\mathbf{p}_f = \mathbf{p}_i + \hbar\mathbf{Q}$ (Fig. 5). The approximation that the neutrons scatter from a collection of free atoms is termed the impulse approximation (IA). The dynamic structure factor in the impulse approximation is given by

$$S_{\text{IA}}(Q, \omega) = \frac{1}{\rho} \int \frac{d^3\mathbf{p}_i}{(2\pi\hbar)^3} n(\mathbf{p}_i) \delta(\hbar\omega - E_{p_f} + E_{p_i}), \quad (2)$$

where ρ is the density of the liquid helium, $E_p = p^2/2m$, m is the mass of the helium atom, and the delta function is an expression of energy conservation. Note that $S_{\text{IA}}(Q, \omega)$ is normalized so that its integral over $\hbar\omega$ is unity at large Q .

The important feature of the impulse approximation is that it provides the desired simple relation between the neutron scattering law for helium and its momentum distribution. But how do we know whether an experiment has been performed at conditions for which the impulse approximation is valid? Equation 2 implies that, at a given value of Q , a plot of the observed $S(Q, \omega)$ versus ω should have a single peak that is symmetric about the recoil energy of an atom at rest, $\hbar\omega_{\text{recoil}} = E_{\hbar Q}$.



KINEMATICS FOR IMPULSE APPROXIMATION

Fig. 5. According to the impulse approximation, neutron scattering from liquid ${}^4\text{He}$ can be regarded, at sufficiently high momentum and energy transfers, as scattering from free atoms. That situation is depicted here schematically. Arrows represent the momenta of a neutron and a helium atom before and after scattering. The dashed line represents the momentum $\hbar\mathbf{Q}$ and energy $\hbar\omega$ transferred to the helium atom during the scattering. Momentum conservation demands that $\mathbf{p}_f = \mathbf{p}_i + \hbar\mathbf{Q}$, where \mathbf{p}_i and \mathbf{p}_f are, respectively, the initial and final momenta of the helium atom. Because the binding energy of the helium atoms is ignored in the impulse approximation, the difference between the energies of a helium atom before and after scattering is simply equal to the difference in its kinetic energies before and after scattering, $(1/2m)(p_f^2 - p_i^2)$. Furthermore, energy conservation requires that $(1/2m)(p_f^2 - p_i^2) = \hbar\omega$.

Moreover, since $\hbar\omega - E_{p_i} + E_{p_i} = \hbar\omega - \hbar\omega_{\text{recoil}} - \mathbf{Q} \cdot \mathbf{p}_i/m$, the peak width should be proportional to Q times the width of the momentum distribution.

In the presence of a Bose condensate, the initial momentum distribution should have the form

$$n(\mathbf{p}_i) = n_0 \rho (2\pi\hbar)^3 \delta^{(3)}(\mathbf{p}_i) + n^*(\mathbf{p}_i), \quad (3)$$

where $\delta^{(3)}(\mathbf{p}_i)$ is a three-dimensional delta function and $n^*(\mathbf{p}_i)$ is a smooth momentum-distribution function for the remainder of the atoms. Combining Eqs. 2 and 3 yields a unique form for the dynamic structure factor in the impulse approximation:

$$S_{IA}(Q, \omega) = n_0 \delta(\hbar\omega - \hbar^2 Q^2/2m) + S_{IA}^*(Q, \omega), \quad (4)$$

where $S_{IA}^*(Q, \omega)$ is the contribution to the scattering law from $n^*(\mathbf{p}_i)$. A Bose-condensate peak in the momentum distribution should show up as a delta function in the observed $S(Q, \omega)$ at $\hbar\omega = E_{\hbar Q}$, and n_0 should equal the fraction of the integral of the observed $S(Q, \omega)$ over $\hbar\omega$ contributed by the delta function. It is this simple prediction that has motivated the condensate saga, that is, the many attempts to observe the condensate by neutron-scattering experiments.

More generally, the impulse approximation, which assumes the helium atoms scatter neutrons as if they are free particles, predicts that the scattering is no longer a function of ω and Q separately. Rather, the energy-conservation delta function in Eq. 2 forces a relationship between ω , Q , and k_{\parallel} , the component of an atom's initial wave vector parallel to the direction of the momentum transfer: $k_{\parallel} = (m/\hbar^2 Q)(\hbar\omega - \hbar^2 Q^2/2m)$. To express this fact we can introduce a new variable Y , first suggested by Geoffrey West:

$$Y \equiv \frac{m}{\hbar^2 Q} \left(\hbar\omega - \frac{\hbar^2 Q^2}{2m} \right). \quad (5)$$

Then we rewrite $S(Q, \omega)$ in terms of a function that depends on Y rather than ω :

$$J(Y, Q) \equiv \hbar^2 Q S(Q, \omega)/m. \quad (6)$$

Equations 5 and 6 are essentially redefinitions (since Y is just a dummy variable and has not been given a physical interpretation) and are therefore valid whether or not the impulse approximation is valid. The quantity $J(Y, Q)$ is termed the *Compton profile* and was used to plot the results of seminal experiments by A. H. Compton and J. DuMond in the 1920s that measured the electron momentum distributions in atoms and metals by x-ray scattering at keV energies. Compton and Dumond plotted their results in terms of p_{\parallel} , but, because the impulse approximation was valid in their experiments, p_{\parallel} is identically equal to $\hbar Y$.

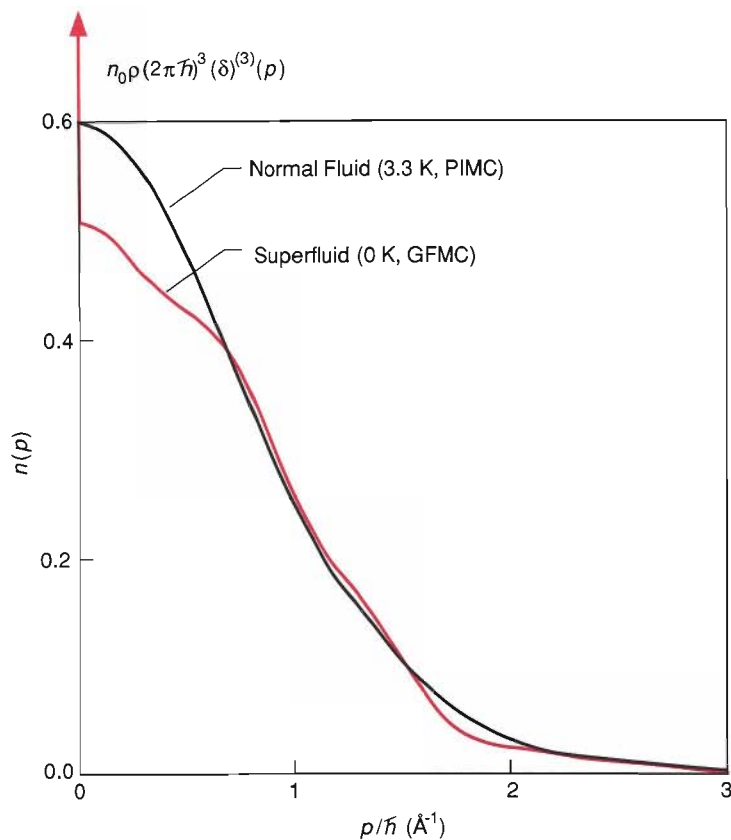
The advantage of expressing scattering laws as Compton profiles is that, in the impulse approximation, $J(Y, Q)$ depends only on Y and not on Q , a phenomenon we refer to as *Y-scaling*. In particular the Compton profile for liquid helium in the impulse approximation is given by

$$J_{IA}(Y) = n_0 \delta(Y) + \frac{1}{4\pi^2 \rho} \int_{|Y|}^{\infty} dk kn(k). \quad (7)$$

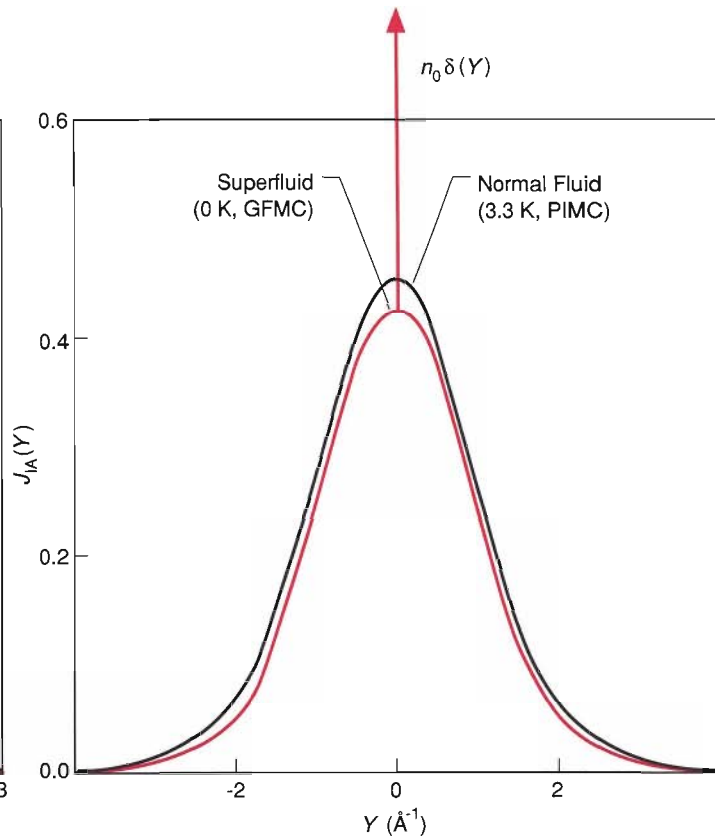
Note that the momentum distribution in Eq. 7 depends only on the magnitude of \mathbf{k} because the liquid is isotropic. If the impulse approximation is valid, then it should be possible to extract n_0 and $n(k)$ from neutron scattering experiments by direct inversion of Eq. 7.

We will now examine whether conditions for the impulse approximation, which implies *Y-scaling*, have been met experimentally. We will also consider the possibility, first suggested by West, that *Y-scaling* is independent of the validity of the im-

(a) Momentum Distributions



(b) Compton Profiles



pulse approximation. In other words, even when conditions for the impulse approximation are not met, the Compton profile may still depend only on Y . Scaling phenomena are of intense interest throughout modern physics, for they occur whenever the number of variables involved in a measurement on a physical system exceeds the number of relevant length or energy scales for the system. Thus, observation of scaling is indicative of a fundamental simplicity of the physical system being studied. In the case of high-energy neutron scattering from helium, the number of relevant variables might, in principle, be on the order of 10^{23} , the number of atoms in a typical sample. Observation of Y -scaling would indicate that the number of relevant variables has been reduced to one. In the impulse approximation the relevant variable is k_{\parallel} , and it determines the scattering through the momentum distribution. Later when we discuss corrections to the impulse approximation due to final-state effects, we will present a theory in which the scattering law obeys Y -scaling but Y does not equal k_{\parallel} and has an alternative interpretation.

Theoretical Predictions

To advance from qualitative arguments to quantitative predictions for neutron-scattering experiments, we need to consider the theoretical predictions for momentum distributions that are used as input to the impulse approximation. A wide variety of many-body calculational methods have been developed and applied to calculate the momentum distributions in helium. Remarkably, the most straightforward method, which involves perturbative expansion in the potential about the non-interacting ground state using Feynman-diagram (field-theory) methods, works poorly for helium. The reason is that the He-He potential (Fig. 3a) is singular (infinite) at short distances. Thus, an infinite-order resummation of the perturbative expansion is required in order to obtain nonsingular answers. (We return to this point in the sidebar “How Final-State Effects Were *Really* Calculated.”) However, several

PREDICTION OF BOSE CONDENSATE BY *AB INITIO* THEORY

Fig. 6. (a) An *ab initio* calculation of the momentum distribution $n(p)$ in superfluid helium at absolute zero (red curve) exhibits a delta-function spike at $p = 0$, which is interpreted as the signature of a Bose-condensate fraction in the superfluid of about 9.24 percent. As expected, an *ab initio* calculation of $n(p)$ in normal-fluid helium at 3.3 kelvins lacks a delta-function spike at $p = 0$. The acronyms GFMC and PIMC refer to calculational methods described in the text. (b) The theoretical Compton profiles $J_{IA}(Y)$ shown here were calculated by using the theoretical momentum distributions as input to the impulse approximation. The integral over Y of each Compton profile is unity. The fraction of the integral of the 0.32-kelvin $J_{IA}(Y)$ contributed by its delta-function spike is the Bose-condensate fraction at that temperature.

methods have been developed that avoid the pathologies of perturbative expansions for strong potentials.

One approach is to invoke a quantum-mechanical variational principle that allows one to calculate the momentum distribution by minimizing the energy of trial wave functions for the ground state of ${}^4\text{He}$. The most successful of such variational methods is the *hypernetted chain* (HNC) approximation. Another approach, termed the *Green's function Monte Carlo* (GFMC) method, is to use a stochastic Monte Carlo algorithm to solve the many-body Schrödinger equation for the ground-state wave function. A third approach, termed the *path-integral Monte Carlo* (PIMC) method, is to invoke the path-integral formulations of quantum mechanics and statistical mechanics originally proposed by Feynman to solve for the momentum distribution as a sum over classical paths in imaginary time. The path-integral method is especially applicable to nonzero temperatures, whereas the variational and Green's function methods, which calculate the ground-state wave function, yield the momentum distribution at zero temperature only.

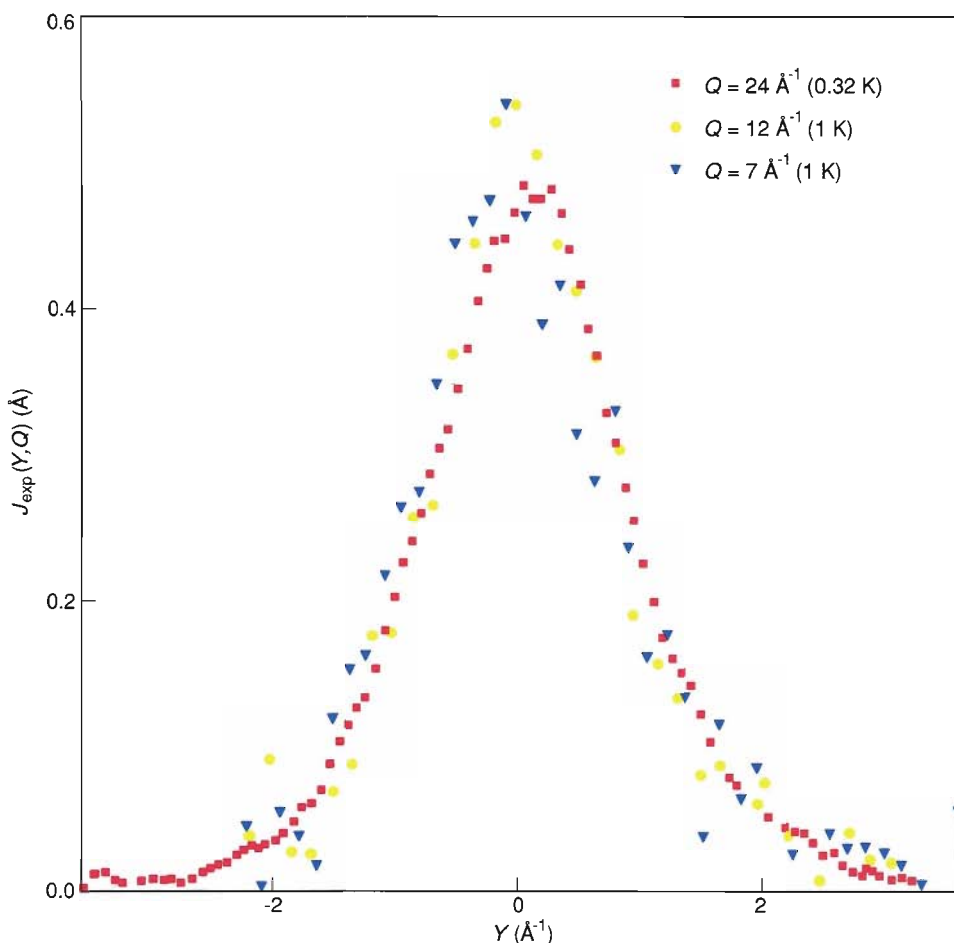
Figure 6a shows the momentum distribution predicted by the GFMC method for superfluid ${}^4\text{He}$ at absolute zero and the momentum distribution predicted by the PIMC method for normal-fluid ${}^4\text{He}$ at 3.3 kelvins. The GFMC method yields a delta function in the zero-temperature momentum distribution at $p = 0$ corresponding to a Bose-condensate fraction of 9.2 percent, much less than the non-interacting value of 100 percent. (The HNC method also yields a delta function at $p = 0$ and the same value for n_0 .) The PIMC calculation, which has been carried out only for $T > 1$ kelvin, shows a condensate fraction that tends toward the GFMC and HNC value at the lowest temperature calculated and tends toward zero as the temperature approaches T_λ . At $T \geq T_\lambda$ the PIMC method yields a momentum distribution that is smooth and approximately Gaussian, as seen in Fig. 6a for $T = 3.3$ kelvins. The widths of all these momentum distributions are roughly equal to the $\Delta k \approx 2 \text{ \AA}^{-1}$ that we estimated heuristically from examination of the He-He potential and the pair-correlation function for liquid ${}^4\text{He}$.

Using the GFMC and the PIMC momentum distributions of Fig. 6a to calculate the Compton profiles in the impulse approximation yields the theoretical predictions for $J_{\text{IA}}(Y)$ shown in Fig. 6b. Note that a delta-function peak at $Y = 0$ is predicted for the superfluid at temperatures below T_λ , whereas a smooth $J_{\text{IA}}(Y)$ is predicted for the normal fluid at temperatures above T_λ .

Experimental Results

The critical experimental issue for momentum-distribution measurements is to achieve conditions at which the impulse approximation may be valid, namely, high values of Q and ω . To do so requires neutrons with relatively high energies, on the order of hundreds of meV. Because the spectrum of neutrons from a reactor is a Maxwell-Boltzmann distribution that peaks at 23 meV, the neutron flux decreases exponentially with further increases in energy. Therefore, reactor experiments are generally limited to Q values less than 12 \AA^{-1} . Many experiments on ${}^4\text{He}$ have been done at reactor sources, and the most carefully analyzed data lie in the Q range between 4 \AA^{-1} and 7 \AA^{-1} . However, in this Q range the deviations from the impulse approximation are large.

More recently, experiments have also been done at pulsed neutron sources. In order to maintain short pulse widths for time-of-flight experiments, pulsed neutron sources have an undermoderated neutron spectrum; that is, a relatively large fraction of the neutrons fail to reach a thermal distribution before they exit the moderator. Thus, the flux of high-energy neutrons decreases only inversely with increasing energy, so higher energy and momentum transfers are achieved. In 1986 a team headed by Paul Sokol of The Pennsylvania State University organized an effort to build a



Y-SCALING OF MEASURED COMPTON PROFILES FOR SUPERFLUID ^4He

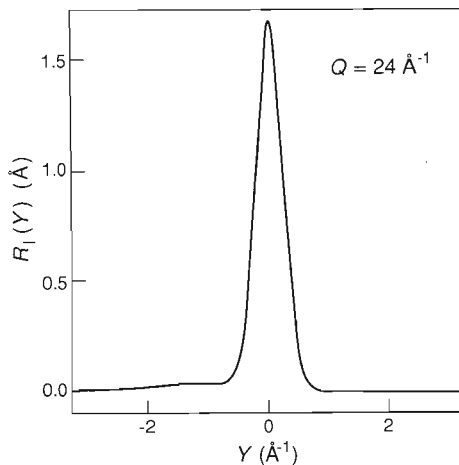
Fig. 7. Each of the measured Compton profiles, $J_{\text{exp}}(Y, Q)$, for superfluid ^4He shown here is broadened by a Gaussian instrumental resolution function with a full width at half maximum of about 0.6 \AA^{-1} . The $7\text{-}\text{\AA}^{-1}$ and the $12\text{-}\text{\AA}^{-1}$ data were taken at a reactor, and the $24\text{-}\text{\AA}^{-1}$ data were taken at a pulsed neutron source. Note that each data set lies approximately on the same curve irrespective of the Q value at which it was obtained. In other words, the measured Compton profiles exhibit the Y -scaling predicted by the impulse approximation. Also note that small deviations from the impulse approximation, in the form of an asymmetry in the peak shape and a leftward shift of the peak center, are visible in the $7\text{-}\text{\AA}^{-1}$ data.

chopper spectrometer optimized for momentum-distribution studies. The spectrometer, known as Phoenix, was built at the Intense Pulsed Neutron Source at Argonne National Laboratory. Phoenix has provided data at Q values up to 24 \AA^{-1} . The pulsed-source experiments thus more closely approach conditions at which the impulse approximation might be valid. They also permit much greater control of the instrumental resolution function than do reactor experiments.

Figure 7 shows experimental data for the Compton profile of superfluid ^4He . (The $7\text{-}\text{\AA}^{-1}$ and $12\text{-}\text{\AA}^{-1}$ data were obtained at a reactor source and the $23\text{-}\text{\AA}^{-1}$ data were obtained at a pulsed neutron source. Each data set is broadened by an approximately Gaussian instrumental resolution function with a full width at half maximum, ΔY_{FWHM} , of about 0.6 \AA^{-1} .) At first glance all the data sets look symmetric and centered at $Y = 0$. Moreover, the widths and shapes of the $J_{\text{exp}}(Y, Q)$ appear to be independent of Q , in agreement with our expectations for Y -scaling of the Compton profile. The width not only fits our heuristic estimate of 2 \AA^{-1} , which was based on a consideration of zero-point energies, but also is comparable to the prediction of *ab initio* theory (see Fig. 6b).

However, a more careful examination reveals some discrepancies with this simple picture. Note that the $7\text{-}\text{\AA}^{-1}$ data are slightly asymmetric and the peak center is shifted to the left of $Y = 0$. The asymmetry is still present but smaller in the $12\text{-}\text{\AA}^{-1}$ data and is smallest in the $23\text{-}\text{\AA}^{-1}$ data. Additional reactor data at $Q \leq 12 \text{ \AA}^{-1}$ show that the width of the peak does not remain constant but rather oscillates about an average value as Q increases. These observations call into question the validity of the impulse approximation for the reactor Q range. Moreover, no reactor experiment has shown a well-resolved delta-function peak due to a Bose condensate.

Heretofore the above discrepancies have been minimized by data-analysis procedures that include symmetrizing the data and averaging over several Q . The data-



INSTRUMENTAL RESOLUTION FUNCTION FOR PHOENIX

Fig. 8. The chopper spectrometer known as Phoenix is located at the Intense Pulsed Neutron Source at Argonne National Laboratory. Its instrumental resolution function, $R_I(Y)$, at $Q = 24 \text{ \AA}^{-1}$ was calculated by a Monte Carlo simulation and checked by experiments on samples whose scattering is well documented. Theoretically predicted Compton profiles must be convolved with $R_I(Y)$ before being compared with Phoenix data.

analysis procedures have assumed that some additional unknown mechanism broadens the impulse approximation and thereby broadens the delta function that would be produced by the Bose condensate. To determine the Bose-condensate fraction, the data are fit to a model for the momentum distribution in which n_0 is the only free parameter, and data at $T > T_\lambda$ are used to fix the momentum distribution for the remainder of the atoms. Some authors claimed that these procedures lead to a value for the condensate fraction of about 10 percent. The rune in the opening illustration of this article was drawn in 1983 to celebrate those claims and the seventy-fifth jubilee of the discovery of liquid helium. However, the data-analysis procedures leading to the claims had a serious conceptual error. The most credible value for n_0 obtained by model-fitting procedures is between 4 and 5 percent, in serious disagreement with *ab initio* calculations of momentum distributions. That is where the condensate saga stood in 1986 when we entered the picture.

As mentioned earlier, three new elements have converged to resolve the question of the momentum distributions in ^4He . First, instruments at pulsed neutron sources have yielded more accurate data at higher Q values. Second, highly accurate many-body calculations of momentum distributions have become feasible on supercomputers. And third, a new theory for the broadening of the impulse approximation due to final-state effects has been developed by this author. The new theory of final-state effects eliminates model fitting and permits a direct comparison between *ab initio* theory and experiment.

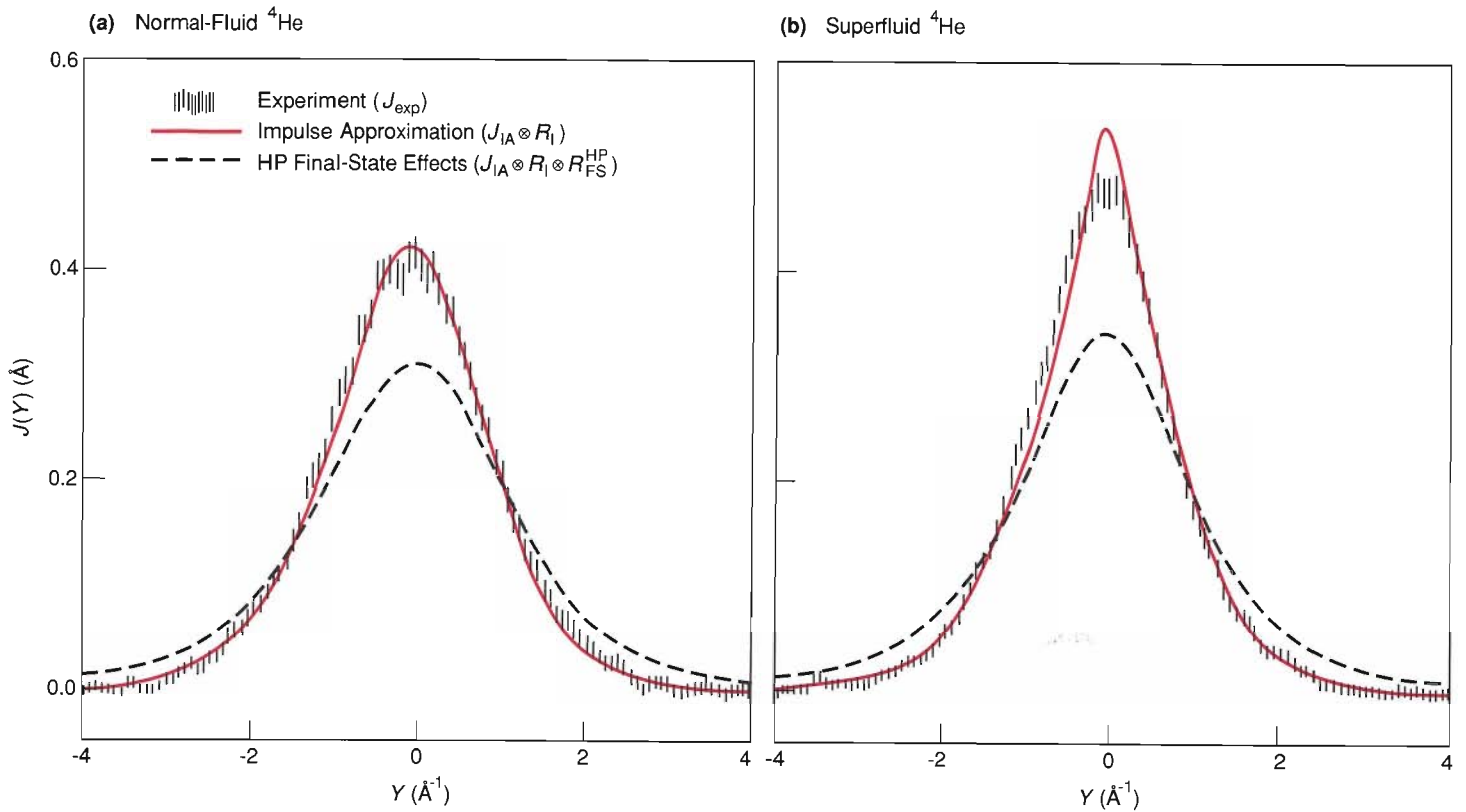
Before discussing final-state effects, we need to show more clearly the discrepancies between theory and experiment. The best data for comparison with theory is the pulsed-source data of Sosnick, Snow, Sokol, and Silver obtained at $Q = 24 \text{ \AA}^{-1}$ with the Phoenix instrument. To compare theory with the measured Compton profile, we must first determine the instrumental resolution function of the spectrometer, $R_I(Y)$. We used a Monte Carlo simulation of the Phoenix spectrometer to calculate $R_I(Y)$; the result (Fig. 8) was confirmed by experiments on samples whose scattering is well known. We then convolve $R_I(Y)$ with the theoretical Compton profile, $J(Y, Q)$, to obtain a prediction for $J_{\text{exp}}(Y, Q)$, the measured Compton profile:

$$J_{\text{exp}}(Y, Q) = R_I \otimes J \equiv \int_{-\infty}^{\infty} dY' R_I(Y - Y', Q) J(Y', Q), \quad (8)$$

where the symbol \otimes denotes *convolution*.

Figure 9a compares theory and experiment for the normal fluid at 3.3 kelvins. The theoretical prediction for $J_{\text{exp}}(Y, Q)$ was calculated by using the PIMC momentum distribution for the normal liquid as input to the impulse approximation and convolving the result with $R_I(Y)$ according to Eq. 8. Despite the absence of adjustable parameters, the agreement between *ab initio* theory and experiment is excellent.

A similar comparison between theory and experiment for the superfluid at 0.32 kelvin is shown in Fig. 9b. The fact that the superfluid data are more sharply peaked around $Y = 0$ than the normal-fluid data suggests changes in the momentum distribution that might be associated with the presence of a Bose condensate. The theoretically predicted $J_{\text{exp}}(Y, Q)$ for the superfluid was calculated by using the GFMC momentum distribution as input to the impulse approximation and convolving the result with $R_I(Y)$. Although the predicted width of $J(Y)$ agrees with experiment, the data are much less sharply peaked in the region around $Y = 0$ than the impulse-approximation prediction. If we now fit the data using the data-analysis procedures previously applied to reactor data, then we might conclude that the Bose-condensate fraction in the superfluid is much smaller than the theoretical value of 9.2 percent. Instead we believe that the discrepancies apparent in Fig. 9b between *ab initio* theory and experiment require corrections to the impulse approximation according to a new theory of final-state effects.



Final-State Effects

The impulse approximation, the basis for all the *ab initio* calculations discussed so far, assumes that the incident neutrons scatter from free helium atoms. In reality, however, after an atom is struck by a neutron, it interacts with neighboring atoms in the liquid (see opening illustration). Those interactions, which result in a broadening of the impulse approximation, are called *final-state effects*. Although the last two decades have produced many calculations of final-state effects, the various theories have been controversial and many conflicting results have been published. As a prelude to our recent work on final-state effects, we shall review only those theories that directly contribute to our current understanding.

The earliest and simplest theory of final-state effects was put forward in 1966 by Hohenberg and Platzman. Here we give the heuristic argument leading to their result for final-state broadening. After a helium atom with initial momentum p_i is struck by a neutron, it collides with neighboring atoms at a rate $1/\tau = \rho\sigma_{\text{total}}(Q)\hbar Q/m$, where τ is the average time between collisions, $\sigma_{\text{total}}(Q)$ is the total cross section for scattering of a helium atom with momentum $\hbar Q$ from other helium atoms, and we assume $\hbar Q \gg p_i$. The Heisenberg uncertainty principle implies that the energy of the recoiling atom should have an uncertainty of \hbar/τ . To account for that uncertainty, we alter Eq. 2 by adding to the final neutron energy E_{p_f} an imaginary part called a *self energy*, $\Sigma_{p_f} = -i\hbar/2\tau$. The energy-conserving delta function in Eq. 2, $\delta(\hbar\omega - E_{p_f} + E_{p_i}) \equiv \delta(\Delta E) = (1/2\pi\hbar) \int_{-\infty}^{\infty} dt \exp(it\Delta E/\hbar)$, is replaced by a new delta function:

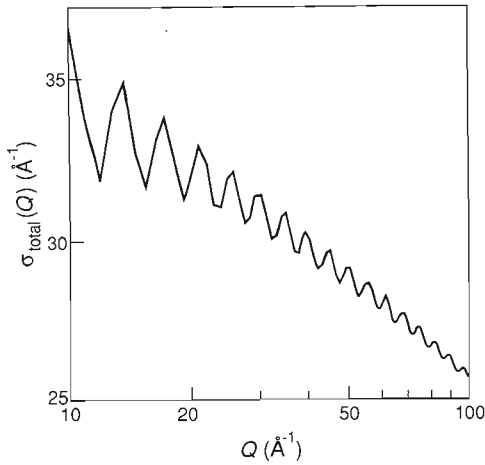
$$\delta(\Delta E - \Sigma_{p_f}) = \frac{1}{2\pi\hbar} \int_{-\infty}^{\infty} dt \exp\left(\frac{it\Delta E}{\hbar} - \frac{i|t|\Sigma_{p_f}}{\hbar}\right). \quad (9)$$

With this replacement it is straightforward to derive that $J(Y, Q)$ is a convolution of the impulse approximation with a broadening function due to final-state effects, $R_{\text{FS}}(Y, Q)$; that is,

$$J(Y, Q) = R_{\text{FS}} \otimes J_{\text{IA}}. \quad (10)$$

EXPERIMENTAL COMPTON PROFILES COMPARED WITH THEORY

Fig. 9. The experimental Compton profiles, $J_{\text{exp}}(Y, Q)$, for (a) normal-fluid ^4He and (b) superfluid ^4He are based on 24-\AA^{-1} Phoenix data obtained at 3.5 kelvins and 0.32 kelvin, respectively. Shown for comparison (solid curves) are the Compton profiles calculated by convolving the predictions of *ab initio* theory and the impulse approximation (Fig. 6b) with the Phoenix instrumental resolution function (Fig. 8). Note that the impulse approximation agrees well with experiment only in the case of normal-fluid ^4He . Also shown (dashed curves) are the Compton profiles calculated by convolving the solid curves with Hohenberg and Platzman's final-state-broadening function, $R_{\text{FS}}^{\text{HP}}(Y)$. Note that the dashed curves deviate substantially from the data.



TOTAL ${}^4\text{He}$ - ${}^4\text{He}$ SCATTERING CROSS SECTION

Fig. 10. The small oscillations, or hard-sphere glories, in this plot of $\sigma_{\text{total}}(Q)$ versus Q are an interference effect due to the symmetry requirement on the two-boson wave function. However, apart from those oscillations the cross section decreases linearly with $\ln Q$. As a result, the neutron scattering law also has a logarithmic dependence on Q at large Q and thus approaches the impulse approximation (which is independent of Q) only very slowly (see Fig. 13).

The final-state broadening function should have a Lorentzian form:

$$R_{\text{FS}}(Y, Q) = \frac{1}{\pi} \frac{\Gamma}{Y^2 + \Gamma^2},$$

where

$$\Gamma = \frac{1}{2} \rho \sigma_{\text{total}}(Q). \quad (11)$$

As we will see later, many features of this early theory coincide with our current model of final-state broadening. For example, both models predict that the full width at half maximum of the broadening has the form

$$\Delta Y_{\text{FWHM}} \approx \rho \sigma_{\text{total}}(Q). \quad (12)$$

Moreover, if the potential is infinitely steep (*hard core*) and thus $\sigma_{\text{total}}(Q)$ is independent of Q , the final-state-broadened $J(Y, Q)$ of the Hohenberg and Platzman model obeys Y -scaling even if the impulse approximation is not applicable, a result in accord with the original suggestion of West and a feature of our model also. Unfortunately, nature has not been so kind: We see in Fig. 10 that, instead of being constant, $\sigma_{\text{total}}(Q)$ is a logarithmic function of Q (apart from small *glory* oscillations, which are an interference effect due to the Bose-Einstein spin-statistics relation). The logarithmic dependence of $\sigma_{\text{total}}(Q)$ reflects the steepness of the He-He potential at short distances (see Fig. 3a). It also implies that even at very high Q the impulse approximation cannot be applied directly. Instead Y -scaling is approximately true (the deviations vary as $\ln Q$), and corrections for final-state effects must be made.

Although the Hohenberg and Platzman model shares many features with our present model, it is not completely correct for two reasons. First, the exact *kinetic-energy sum rule* (ω^2) on $S(Q, \omega)$ requires that, at high Q ,

$$\int_{-\infty}^{\infty} dY Y^2 R_{\text{FS}}(Y, Q) = 0. \quad (13)$$

That is, final-state effects should not affect the second moment, or Gaussian width, of $J(Y, Q)$. The form for $R_{\text{FS}}(Y, Q)$ given in Eq. 11 does not satisfy the kinetic-energy sum rule and, in fact, yields an infinite value for the integral in Eq. 13. Second, the broadening predicted by Eq. 11 is much larger than is observed experimentally. For example, Fig. 9a shows that convolution of the Hohenberg-Platzman broadening function with the PIMC impulse-approximation prediction for the normal fluid yields a $J(Y)$ that is in serious disagreement with the data.

The additional qualitative physics required to complete the theory for final-state effects was first proposed by Gersch and Rodriguez in 1973, but their results were ignored in more than twenty subsequent theoretical papers on final-state effects as well as in the many papers analyzing the reactor experiments. In 1987 this author independently developed a theory embodying the same qualitative physics but implying new many-body techniques (see “How Final-State Effects Were *Really* Calculated”). The new theory predicted exactly the results obtained soon after from the new pulsed-source experiments.

Here we present a heuristic description of the new theory. As discussed earlier, the atoms in liquid ${}^4\text{He}$ are not uniformly distributed in space; rather they are distributed according to the pair-correlation function shown in Fig. 4. At Q values of many \AA^{-1} , the motion of an atom recoiling from a neutron collision can be described heuristically by a classical trajectory. Figure 3b shows that initially an atom is likely to be in the attractive part of the potential and that, after being struck by a neutron, the atom travels for some distance before it begins to collide with the

steeply repulsive cores of the potentials of neighboring atoms. The collision rate, $1/\tau$, depends on the recoil distance $x = \hbar Q/m$: $1/\tau(x) \approx \rho g(x) \sigma_{\text{total}}(Q) \hbar Q/m$. Since $g(x)$ is zero at small x , there will be no scattering at short recoil times. Also, since $g(x)$ approaches unity at large x , the scattering rate should approach the Hohenberg and Platzman prediction at long recoil times. With this reasoning we deduce that the self energy to be used in Eq. 9 depends on the recoil distance; that is, $\Sigma_{pr}(x) = -i\hbar/2\tau(x)$. The result for the final-state broadening then becomes

$$R_{\text{FS}}(Y, Q) \approx \frac{1}{2\pi} \int_{-\infty}^{\infty} dx \exp[iYx - |x|g(|x|)\Gamma], \quad (14)$$

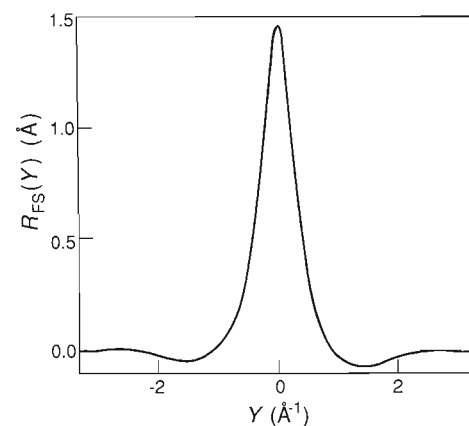
where again $\Gamma = \frac{1}{2}\rho\sigma_{\text{total}}(Q)$. The Hohenberg and Platzman prediction, Eq. 11, can be obtained from Eq. 14 in the limit of a structureless fluid ($g(r) \rightarrow 1$). However, unlike Eq. 11, Eq. 14 satisfies the kinetic-energy sum rule because, in fact, $g(0) = 0$. Note also that the broadening given by Eq. 14 has the same FWHM as the broadening of Hohenberg and Platzman, but it is negative at large $|Y|$ in order to satisfy the sum rule. A somewhat more accurate field-theoretic version of the new theory is discussed in the sidebar.

In the new theory the scaling variable, Y , acquires a new physical interpretation as the variable conjugate to the distance traveled by a recoiling atom. In the limit of a hard-core potential (that is, $\sigma_{\text{total}}(Q) = 2\pi r_0^2$, where r_0 is the hard-core radius and the factor of 2 accounts for forward diffractive scattering), final-state effects become a geometric problem that depends only on r_0 and the relative atomic positions given by $g(r)$. In quantum mechanics the position of an atom, in this case the recoil distance x , is not a variable distinct from its momentum. Rather, they are conjugate variables in the sense of a Fourier transform. Hence, introducing the relative positions of the atoms introduces no new variables into the problem, and Y -scaling will continue to hold even though the impulse approximation does not. Remember, all this assumes σ_{total} is independent of Q . If we now include the Q dependence of $\sigma_{\text{total}}(Q)$, we have indeed introduced a new variable and Y -scaling breaks down. However, since in practice $\sigma_{\text{total}}(Q)$ varies approximately as $\ln Q$, the corrections to Y -scaling in our theory are logarithmic, that is, slowly varying with Q .

Figure 11 shows the final-state broadening function predicted by the somewhat more sophisticated version of our theory presented in the sidebar. To make experimental predictions we must convolve $J_{\text{IA}}(Y)$ with the $R_{\text{FS}}(Y, Q)$ of Fig. 11 and with the $R_1(Y, Q)$ of Fig. 8. The results for the normal fluid and the superfluid are shown, together with the pulsed-source data, in Figs. 12a and 12b, respectively. The agreement between theory and experiment is now excellent for both the normal fluid and the superfluid! Experiment and theory both converge to a Bose-condensate fraction in the superfluid of 9.2 percent. We emphasize that the many-body calculations of momentum distributions and the theory for final-state effects were completed before the pulsed-source experiments were performed, so that in this case *ab initio* theory accurately predicted experiment. Further experiments by Sokol and collaborators show excellent agreement over the entire quantum-liquid region of the phase diagram of ^4He and at a variety of Q .

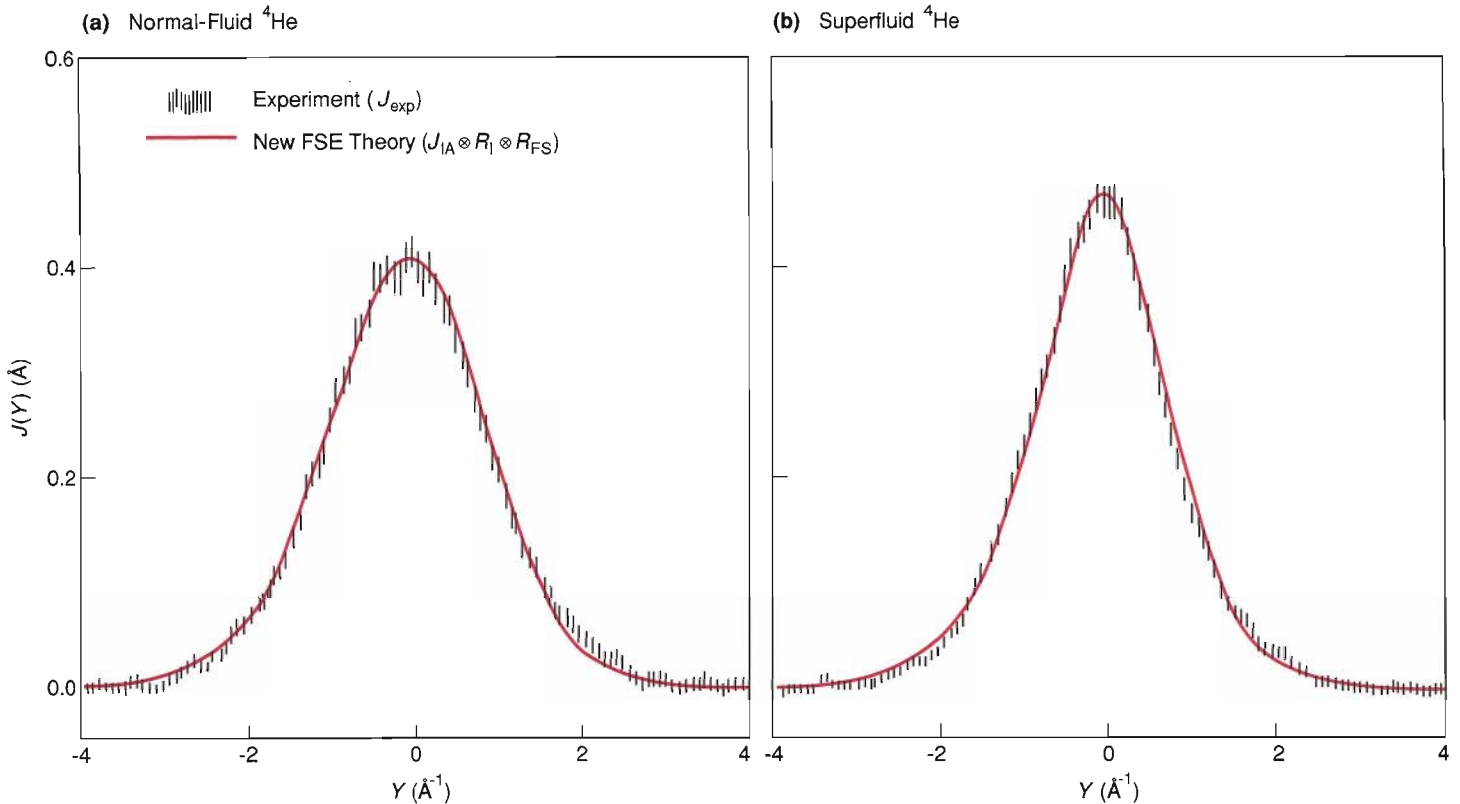
Implications of the Breakthrough

The convergence of theoretical and experimental routes to the momentum distributions of ^4He has finally confirmed London's fifty-year-old hypothesis connecting superfluidity with the existence of a Bose condensate—and may thus be considered a triumph for modern condensed-matter physics. The success of the momentum-distribution calculations provides confidence in the new supercomputer calculational methods for many-body quantum systems. The new theory of final-state effects points



BROADENING FUNCTION PREDICTED BY NEW FSE THEORY

Fig. 11. Shown here is the broadening function, $R_{\text{FS}}(Y)$, predicted by the author's new theory of final-state effects (FSE). The full width at half maximum of $R_{\text{FS}}(Y)$, like that of Hohenberg and Platzman's final-state-broadening function, is given approximately by $\rho\sigma_{\text{total}}(Q)$. However, $\int_{-\infty}^{\infty} dY Y^2 R_{\text{FS}}(Y) = 0$, and thus, unlike Hohenberg and Platzman's final-state-broadening function, $R_{\text{FS}}(Y)$ satisfies the exact kinetic-energy sum rule on the neutron scattering law.



CONVERGENCE OF THEORY AND EXPERIMENT

Fig. 12. Convolution of the impulse approximation (Fig. 6b) with the broadening function given by the author's final-state-effects theory (Fig. 11) yields predicted Compton profiles that agree well with the data for both (a) normal-fluid ^4He and (b) superfluid ^4He . The agreement for normal-fluid ^4He arises because the sum rule satisfied by the new final-state broadening function ensures that final-state effects do not change the width of the normal fluid's essentially Gaussian momentum distribution. In the case of superfluid ^4He , both theory and experiment yield a Bose-condensate fraction of about 9.24 percent.

toward novel perturbative methods for calculating the dynamical response of strongly correlated systems (see sidebar). And the success of the experiments with the Phoenix spectrometer demonstrates the utility of high fluxes of epithermal neutrons in measuring quantities of fundamental scientific importance. However, the convergence does not mean that the condensate saga is finally at an end. Like many research breakthroughs, this one has important implications for future research.

If the *ab initio* calculations of momentum distributions in ^4He are correct, the data are consistent with no other theory for final-state effects except that of the author. Thus we believe that the new theory, or improved versions thereof, can be used with confidence to interpret and predict future experiments on momentum distributions in condensed-matter systems. The fact that the new theory predicts much smaller final-state effects than those predicted by Hohenberg and Platzman is encouraging. However, the theory also tells us that final-state broadening washes out sharp structure in the momentum distribution and that, because $\Delta Y \propto \sigma_{\text{total}}(Q)$ (see Eq. 12), the broadening decreases only slowly with increasing Q . Figure 13 shows theoretical predictions for $J(Y, Q)$ for increasing values of Q . Note that the broadening in the region near $Y = 0$ decreases, but only slowly, as Q increases from 30 to 270 \AA^{-1} . Thus the theory predicts that the Bose-condensate fraction will not produce a sharp peak in $J(Y)$ in any feasible neutron-scattering experiment. This prediction should be an important test of the new theory.

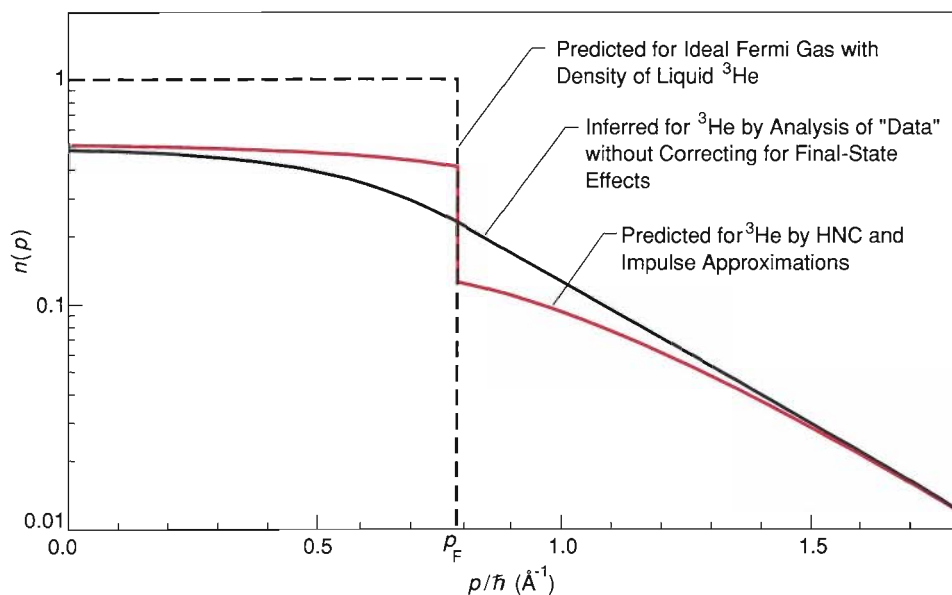
To analyze reactor experiments, the theory will have to be augmented to account for the additional deviations from the impulse approximation that are observed at Q values less than 12 \AA^{-1} . Among those deviations are the oscillations in the width of $J(Y, Q)$ with Q and the asymmetry about $Y = 0$. Both effects may be due to collective behavior in the condensed phase.

Perhaps the most important momentum-distribution experiment to attempt is observation of the Fermi-surface discontinuity in ^3He (that is, the discontinuity in $n(p)$ at $p = p_F$). Figure 14 shows the momentum distribution of a gas of non-interacting fermions with the same density as ^3He . Also shown are the momentum distribution for ^3He predicted by using HNC calculations as input to the impulse approxima-

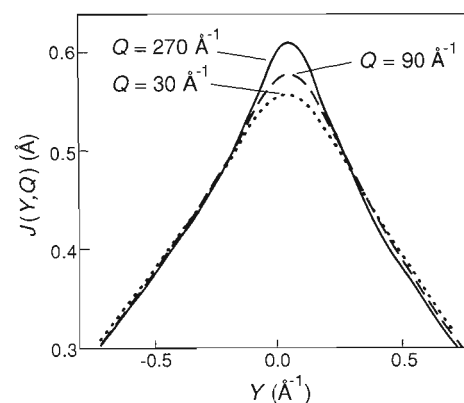
tion and the “apparent” momentum distribution that would be inferred by analyzing final-state-broadened data as if the impulse approximation did not require corrections for final-state effects. In the absence of final-state effects, the discontinuity in $n(p)$ would cause a sharp change in slope in $J_{IA}(Y, Q)$ at $Y = p_F/\hbar$. Unfortunately, the new theory of final-state effects predicts that such a change in slope will not be directly apparent in the data. Nevertheless, experiments can distinguish the HNC theory from other theories that do not have a Fermi-surface discontinuity (such as the pairing theory of Lhuillier and Bouchaud). The HNC theory would predict a different Gaussian width for $J(Y, Q)$ than would other theories. Experiments on ^3He are particularly difficult because ^3He is a strong absorber of neutrons (and is therefore the primary component of thermal-neutron detectors!). Nevertheless, we hope that theory and experiment will resolve the question of the Fermi-surface discontinuity in ^3He in less time than the more than twenty years required to confirm the existence and size of the Bose condensate in ^4He .

At the beginning of this article, we mentioned that ^3He becomes a superfluid at 3 millikelvins. Does that mean a Bose condensate forms in ^3He despite the spin-statistics relation? The answer is no. Superfluidity in ^3He is caused by the formation of Cooper pairs of ^3He atoms and is thus somewhat analogous to superconductivity in metals, which is caused by formation of Cooper pairs of electrons. The difference is that the Cooper pairs of ^3He atoms are uncharged and form a relative p -wave bound state, whereas the Cooper pairs of electrons in metals are charged and usually form a relative s -wave bound state.

The present experimental and theoretical techniques for determining momentum



distributions in helium can also be applied to questions concerning the pressure and temperature dependence of the condensate fraction, the non-existence of a Bose condensate in solid ^4He , the non-existence of a Fermi surface in solid ^3He , the behavior of $n(\mathbf{p})$ at high $|\mathbf{p}|$ (which many-body theories predict is exponential rather than Gaussian even in the normal quantum liquid), the larger n_0 predicted for ^4He in a porous medium (which is expected to behave like a low-density Bose system), the complex momentum distributions expected for mixtures of ^3He and ^4He , the predicted absence of a Bose condensate in the two-dimensional ^4He systems produced by physisorption of ^4He on surfaces, and so on. All such experiments will benefit from the epithermal neutrons provided by pulsed neutron sources or by hot sources at reactors because they all require measurements at high Q values. Although conditions suitable for applying the impulse approximation may never be reached, the final-state corrections will be understood.



CAN THE BOSE CONDENSATE IN ^4He BE OBSERVED DIRECTLY?

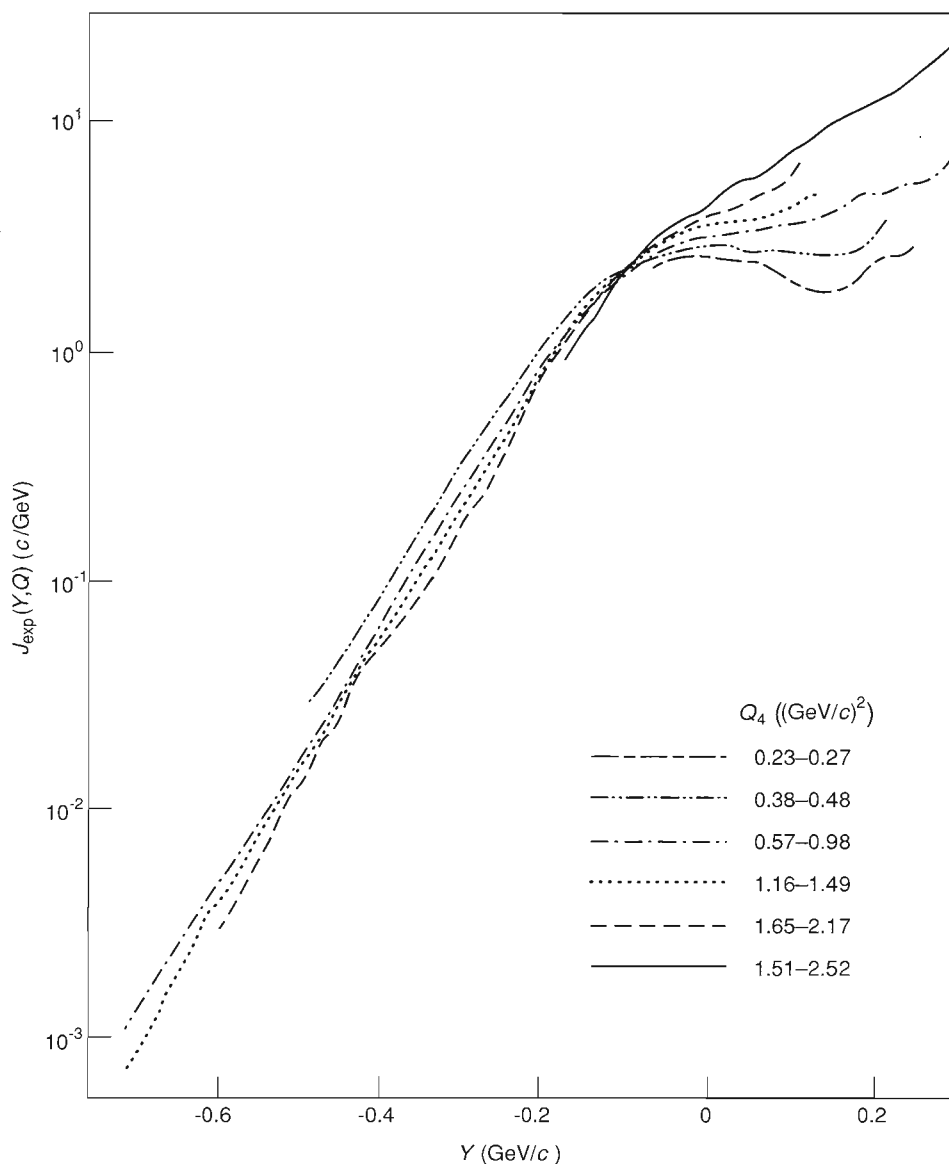
Fig. 13. The author's theory of final-state effects predicts that the Compton profile of ^4He at absolute zero sharpens only slowly with increasing Q near $Y = 0$, the region relevant to the Bose condensate. That prediction implies that the Bose condensate will not produce a distinct peak in the Compton profile at any experimentally feasible Q .

CAN THE FERMI SURFACE IN ^3He BE OBSERVED DIRECTLY?

Fig. 14. The Pauli exclusion principle implies that, at absolute zero, the momentum distribution of an ideal Fermi gas is a step function with a discontinuity of 1 at the Fermi surface, that is, at the momentum of the highest filled momentum state, p_F . Shown here, as a dashed curve, is the absolute-zero momentum distribution of an ideal Fermi gas with the same density as ^3He , for which $p_F/\hbar = 0.789 \text{ \AA}^{-1}$. Also shown, as a red curve, is the absolute-zero momentum distribution predicted for real (interacting) ^3He by the HNC approximation. The discontinuity remains at 0.789 \AA^{-1} , but its magnitude is reduced. Finally, the black curve is the “apparent” momentum distribution, which is inferred as follows. First, the impulse approximation prediction (at 30 \AA^{-1}) obtained by using the red curve as input is convolved with a final-state broadening function appropriate to ^3He . The resulting final-state-broadened “data” are then analyzed by assuming the validity of the impulse approximation but not correcting for final-state effects. Note that the momentum distribution so inferred exhibits no discontinuity at p_F because, like the delta function at $k = 0$ in the momentum distribution of superfluid ^4He , it has been washed out by final-state effects.

Y-SCALING IN ELECTRON-NUCLEON SCATTERING

Fig. 15. Shown here are Compton profiles based on data for the quasi-elastic scattering of electrons from the ^{12}C nucleus at various relativistic four-momentum transfers. The Y variable has been generalized to include relativistic kinematics. The scattering follows Y -scaling for $Y < -0.1 \text{ GeV}/c$, as evidenced by the fact that all the profiles fall on the same curve in that region. Y -scaling breaks down at greater Y values because of excitation of internal degrees of freedom of the nucleons making up the nucleus, such as the $\Delta(1238 \text{ MeV})$ excited state. If final-state effects are ignored, the impulse approximation suggests that the nucleon momentum distribution decreases exponentially with p over nearly four decades. A theoretical explanation for this almost universal behavior is the subject of current research. Determining whether the momentum distribution of helium quantum fluids behave similarly at large p would prove interesting, but the poorer signal-to-noise ratio in neutron-scattering experiments has so far prevented such an experiment.



Going beyond helium, we are now ready to expand our knowledge of momentum distributions to a wide variety of many-body quantum systems. For example, quasi-elastic electron-nucleus scattering (QENS) at GeV energies is aimed at measuring the momentum distributions of nucleons in nuclei. Even though the energy scale characteristic of QENS differs by ten orders of magnitude from the energy scale of neutron scattering from helium, the two types of experiments share many common elements, including Y -scaling phenomena, the importance of final-state effects, and the methods for calculating properties of the many-particle wave functions. Figure 15 shows $J(Y, Q)$ for electron scattering from the ^{12}C nucleus. For $Y \leq 0$ the Compton profile exhibits a relativistic analogue of Y -scaling over nearly four orders of magnitude in $J(Y, Q)$. For $Y \geq 0$ excitation of internal degrees of freedom of the nucleons, such as the $\Delta(1238 \text{ MeV})$ resonance, destroys the Y -scaling. Note also the nearly exponential dependence of $J(Y, Q)$ on $|Y|$. We do not know whether the exponential dependence is a property of the underlying momentum distribution or is a manifestation of final-state effects. That question has been as important in nuclear physics as the existence of a Bose condensate in helium. Thus we plan to make the extension of our final-state theory to nuclei a high priority. ■

How final-state effects were *really* calculated

The derivation of final-state broadening presented in the main text was physically intuitive but, like all heuristic arguments, involved a sleight of hand:

The classical-trajectory concept was not derived from first principles. In practice, the theory of final-state effects is a very difficult many-body problem. Conventional perturbative expansion about the non-interacting ground state, a technique so successful in calculating the properties of weakly interacting systems, is not a useful approach here because helium atoms interact at short distances through a steeply repulsive potential. However, alternatives to perturbation methods, such as the variational and Monte Carlo methods, are capable of handling strongly interacting systems and thus have been most successful in calculating ground-state properties of helium, including the momentum distribution $n(p)$ and the pair-correlation function $g(r)$.

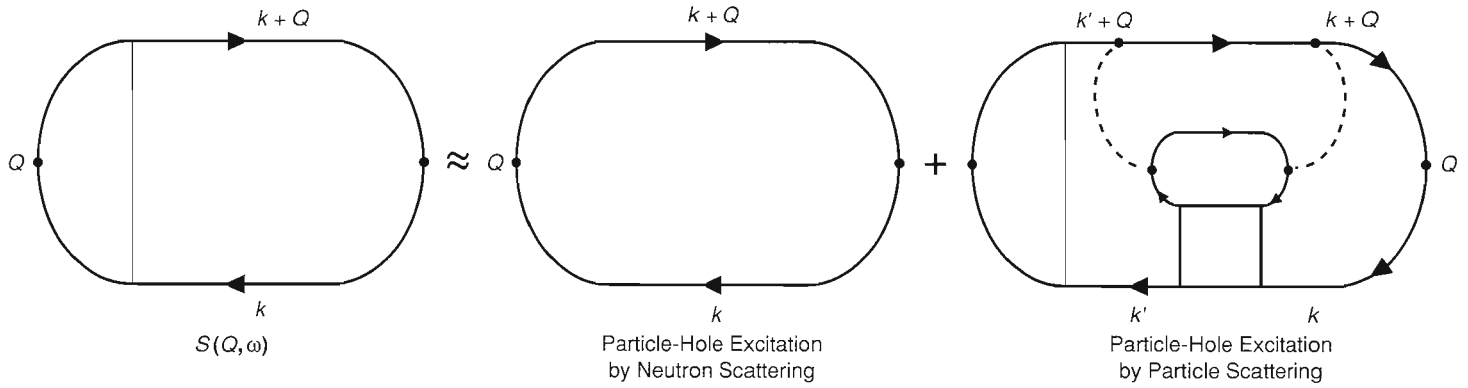
In order to test the ground-state results against neutron-scattering experiments, we need to calculate the dynamical response of the system to neutron scattering. Since we have an obvious interest in not repeating the considerable work involved in generating the ground-state results, we want to calculate the response by applying perturbation theory to the variational and Monte Carlo results for the ground state. However, conventional perturbation theory is again out of the question because the dynamical response also involves helium-helium interactions.

Before we present our solution to this problem, let's outline the starting point. We assume that neutron scattering at momentum transfer $\hbar Q$ introduces, at time zero, a fluctuation about the ground state in the density of atoms with wave vector Q . By calculating the amplitude of that density fluctuation at a later time t and taking its Fourier transform, we can determine $S(Q, \omega)$, the observed scattering law. (Note that ω is conjugate to t .) The density fluctuation is equal to a summation over all so-called particle-hole excitations about the ground state, that is, over all processes that add to the ground state an atom with wave vector $k + Q$ and remove from the ground state an atom with wave vector k .

In the impulse approximation we assume that the particle-hole excitations propagate freely without interacting with other atoms. Final-state effects, on the other hand, are due to interaction of the excitations with other atoms. Scattering of a particle and a hole creates more particle-hole excitations about the ground state. Although in principle an infinity of multiple scatterings of a particle-hole pair can occur, the correlations in the ground-state wave function imply that only single additional particle-hole excitations need be considered. In effect, the correlations screen the steeply repulsive core interaction at short distances, rendering that interaction finite. After all, to minimize their energy in the ground state, the atoms tend to sit in the attractive part of the potential, far away from its steeply repulsive core. Thus the effective final-state interactions can be characterized by a small parameter, and perturbation theory can be used for systematic, controlled calculations.

The divergent terms in the perturbative expansion of $S(Q, \omega)$ involve all processes that transform a $(k + Q, k)$ particle-hole pair to a $(k' + Q, k')$ pair. To obtain finite results, those divergent terms must be explicitly resummed to all orders in the perturbation expansion. In practice, the summation is accomplished by defining a "projection superoperator," which acts in the Hilbert space of $(k + Q, k)$ particle-hole excitations about the ground state much as ordinary operators act in the Hilbert space

Neutron Scattering Law \approx Impulse Approximation + New Final-State-Effects Theory



NEW THEORY OF FINAL-STATE EFFECTS

The author approximates the neutron scattering law for helium as the sum of the impulse approximation and one additional scattering that accounts for final-state effects. Shown here are Feynman diagrams for that approximation. The Feynman diagram for the neutron scattering law represents the propagation of a particle-hole excitation that removes a particle of wave vector k from the ground state and adds to the ground state a particle of wave vector $k + Q$. Arrows denote the direction of momentum flow. Arrows pointing right denote particle lines; arrows pointing left denote hole lines. Only the particle lines carry high momentum. The hatched area denotes the exact result for $S(Q, \omega)$ including all scatterings of particles and holes. The Feynman diagram for the impulse approximation indicates that both particles and holes propagate without scattering. The Feynman diagram for the final-state effects indicates that each particle scatters from another atom and creates a new particle-hole excitation. (Further scatterings are possible but not included in the approximation.) The shaded square is the two-particle density matrix describing the correlations between the two holes in the ground state created by the two particle-hole excitations. The hole-hole correlations are related by sum rules to the pair-correlation function of the ground state. The dashed lines represent the two-particle t -matrix that describes particle scattering. Because the hatched area appears in the Feynman diagrams for both the neutron scattering law and the final-state effects, the scatterings that transform a $(k + Q, k)$ excitation to a $(k' + Q, k')$ excitation must be calculated self-consistently.

of quantum-mechanical states. The neutron scattering law then equals the expectation value of the projection superoperator, and calculations analogous to ordinary perturbation theory can be carried out in the superoperator Hilbert space. The effective interaction is the two-atom scattering matrix multiplied by a ground-state correlation function, which acts to screen the short-distance pathologies of the potential. Additional restrictions on the important scattering processes are obtained by noting that all k entering a two-particle density matrix must be characteristic of the ground-state wave function, as given by the momentum distribution, and that Q is much larger than those characteristic values.

After the above procedure is implemented, the neutron scattering law can be expressed as the sum of the impulse approximation and one additional scattering process. The accompanying figure shows the Feynman diagrams for the components of the sum. In the Feynman diagram for the one additional scattering process, the dashed line represents the t -matrix describing the scattering of two particles and the square represents the two-particle density matrix for the ground state. The latter matrix is a generalization of the correlation functions, such as $g(r)$ and $n(p)$, that characterize the ground-state wave function.

If we approximate the density matrix in terms of $g(r)$ and $n(p)$ in a way that satisfies sum rules and, since Q is large, use a semiclassical approximation for the t -matrix, then the final "Dyson" equation can be solved analytically. The result for the final-state broadening, $R(Y, Q)$, is given by

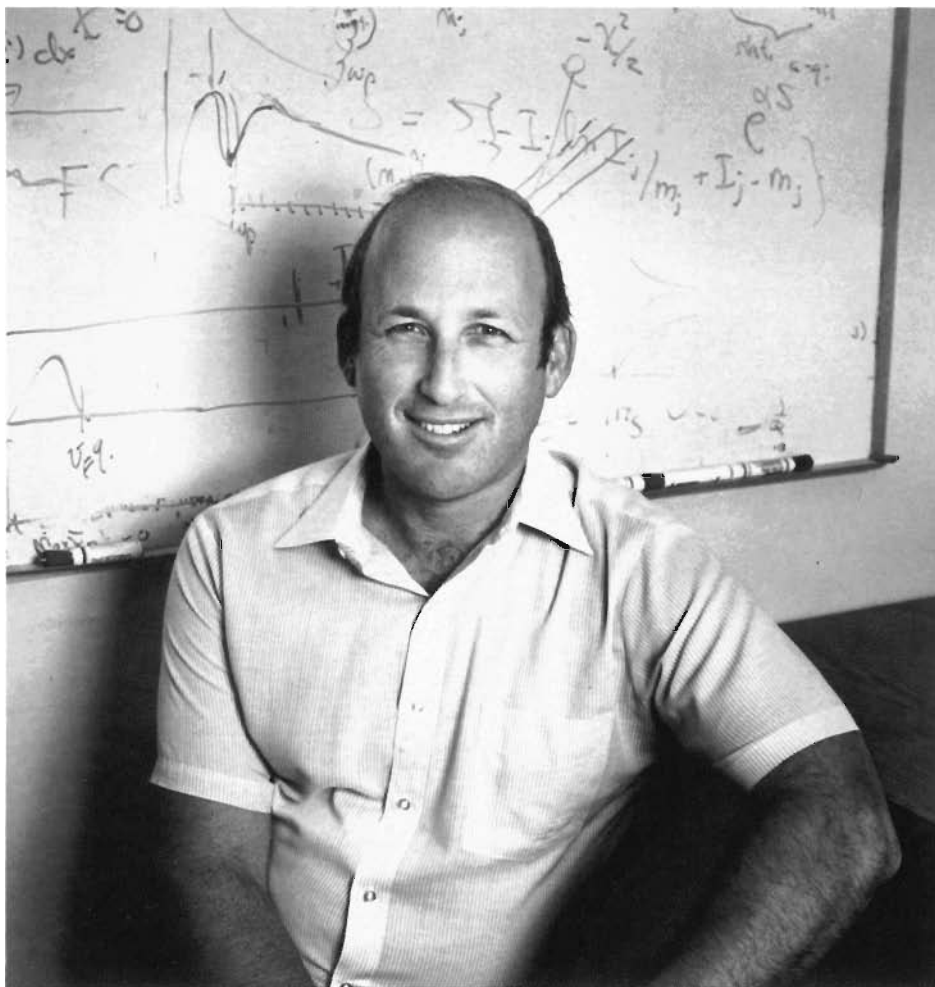
$$R(Y, Q) = \frac{1}{2\pi} \int_{-\infty}^{\infty} dx \exp \left[iYx - \int_0^{|x|} \Gamma(x') dx' \right],$$

where

$$\Gamma(x) = \rho\pi \int_0^{\infty} db^2 (e^{2i\delta_b} - 1) g(\sqrt{x^2 + b^2}).$$

The phase shift δ_b is the semiclassical value for scattering at impact parameter b .

The above expression for $R(Y, Q)$, which is somewhat more complicated than Eq. 14 in the main text, is the expression we have plotted in Fig. 11 of the main text and used in comparing theory with experiment. It is essentially the same as the familiar Wentzel-Kramers-Brillouin (WKB) classical-trajectory approximation taught in elementary quantum mechanics except that the potential, $V(x)$, is replaced by an "optical potential," $\hbar^2 Q \Gamma(x)/m$ that accounts for all repeated scatterings from the same helium atom. The quantity $\hbar^2 Q \Gamma(\infty)/m$ is simply the forward scattering t -matrix for the scattering of two helium atoms. The approach taken here is required for helium, a strong scatterer, but it is satisfying that the result reduces to the WKB approximation in the limit of a weak scatterer. ■



Richard N. Silver received a B.S. in physics (with honors) from the California Institute of Technology in 1966 and a Ph.D. in theoretical physics with a minor in applied mathematics from the same institution in 1971. Then followed a one-year postdoctoral fellowship at Brown University in particle physics and a two-year IBM Postdoctoral Fellowship in Applied Physics at the California Institute of Technology. He joined the Laboratory's Laser Theory Group in 1974, became a founding member of the Condensed Matter and Statistical Physics Group, T-11, in 1977, served as Leader of the Neutron Scattering Group from 1979 to 1986, and since 1986 has held a joint appointment in T-11 and the Los Alamos Neutron Scattering Center. He has organized several conferences and served as a member of several national committees, including the LAMPF Program Advisory Committee and the IPNS Program Advisory Committee. He served as chairman of the Laboratory's Postdoctoral Committee from 1986 to 1989. The results of his research are documented in more than eighty publications on particle physics, semiconductor physics, optical properties of solids, many-body theory, neutron scattering, spectrometer design, maximum entropy and Bayesian methods of statistical inference, and quantum Monte Carlo.

Further Reading

David R. Tilley and John Tilley. 1986. *Superfluidity and Superconductivity*, second edition. Bristol, England: Adam Hilger Ltd. A general introduction to the properties of liquid helium.

Henry R. Glyde and Eric C. Svensson. 1987. Solid and liquid helium. In *Neutron Scattering B*, edited by D. L. Price and K. Skold, 303. Methods of Experimental Physics, volume 23. San Diego: Academic Press, Inc.

Richard N. Silver and Paul E. Sokol, editors. 1989. *Momentum Distributions*. New York: Plenum Publishing Co. A survey of work on momentum distributions in quantum fluids, condensed matter, and nuclei.

R. N. Silver and P. E. Sokol. To be published. Bose condensate in superfluid ^4He and momentum distributions by deep inelastic scattering. In *Recent Progress in Many-Body Theories II*, edited by Y. Avishai. New York: Plenum Publishing Co.

Acknowledgments

The author has benefited from collaborations with several colleagues, especially John Clark of Washington University and Paul E. Sokol of The Pennsylvania State University. Support for the research described in this article was derived from funding of the Los Alamos Neutron Scattering Center by the Division of Materials Science of the DOE Office of Basic Energy Sciences.